Frequency-domain theory of laser infrared photothermal radiometric detection of thermal waves generated by diffuse-photon-density wave fields in turbid media

Andreas Mandelis and Chris Feng
Photothermal and Optoelectronic Diagnostics Laboratories, Department of Mechanical and Industrial Engineering, University of Toronto, Toronto, Canada M5S 3G8
(Received 17 September 2001; published 25 January 2002)

A three-dimensional theory of the frequency-domain thermal-wave field generated inside a turbid medium with optical and thermal properties of human tissue is presented. The optical source is treated as a three-dimensional harmonically modulated diffuse-photon-density wave (DPDW) field in the diffusion approximation of the radiative transfer theory. Unlike earlier Green-function-based theoretical models, exact boundary conditions are used based on the requirement that there should be no diffuse photon intensity entering the turbid medium from the outside. Explicit analytical expressions for the DPDW field and for the dependent thermal-wave field are obtained in the spatial Hankel-transform domain. The formalism is further extended to the calculation of the infrared photothermal radiometric signal arising from the nonradiatively generated thermal-wave distribution in turbid media with instantaneous nonradiative deexcitation as well as in media with nonzero fluorescence relaxation lifetimes. Numerical inversions have been performed and presented as examples of selected special cases of the theory. It is found that the present theory with exact DPDW-field boundary conditions is valid throughout the entire domain of the turbid medium, with the exception of the very near-surface ballistic photon ''skin layer'' (7–50 μm). Photothermal radiometric signals were found to be more reliably predicted than DPDW signals within this layer, due to the depth-integration nature of this detection methodology.

DOI: 10.1103/PhysRevE.65.021909 PACS number(s): 42.66.−p, 87.80.−y, 87.10.+e, 02.60.−x

I. INTRODUCTION

In recent years several noninvasive laser-based diagnostic techniques for tissues have been developed aimed at performing reliable measurements of the optical scattering and absorption properties of healthy and pathological (cancerous) tissue, as well as for imaging purposes. Common to all those techniques is the diffusion (migration) of laser-induced photons in turbid media [1–5]. In particular, pulsed photothermal radiometry (PPTR) is rapidly developing into a very promising tissue diagnostic technique for near-surface applications [6–9] based on the assessment of laser-pulse-induced temperature profiles, with the concomitant extraction of absorption and scattering coefficients. It has been pointed out by Prahl *et al.* [7] that the availability of only a single signal channel, the PPTR transient, makes it difficult to extract reliable (i.e., unique) measurements of both absorption, μ_a, and scattering, μ_s, coefficients of turbid media, without an additional independent optical measurement. This shortcoming tends to compromise the utility of PPTR in tissue diagnostics. Therefore, it is desirable to introduce alternative measurement schemes that will meet the reliability/uniqueness criterion for μ_a and μ_s measurements through the availability of additional signal channels. This can be achieved by means of frequency-domain photothermal radiometry (FD-PTR) [10,11], a technique that provides two signal channels (amplitude and phase). In FD-PTR a harmonically modulated laser beam generates diffuse-photon-density waves in a turbid medium [12,13]. Following photon migration and scattering, the absorbed fraction of the diffusive light wave creates an oscillatory temperature (thermal wave) field, which is detected radiometrically.

In order to interpret experimental data, several theoretical approaches have been taken. The most fundamental approach starts with Maxwell's equations, takes into account the statistical character of turbid media and introduces the statistical moments of the scattered photon wave [14,15]. The mathematical complexities of this exact theory, however, seriously limit its utility in the experimental study of light propagation in turbid media. An alternative approach for multiple-scattering events is that of the radiative transfer theory [14]. Of special appeal is the diffusion approximation to this theory, because of its inherent mathematical tractability. This approximation to electromagnetic wave transport in turbid media is valid in the regime of multiple scattering, such that $\lambda \ll l \ll L$, where λ is the wavelength of light, l is the mean-free path for photon scattering and L is the thickness of the medium [16]. In this (macroscopic) approximation, the multiply scattered intensity is described by means of the diffusion equation. Additional constraints apply, however, which have been investigated extensively by Ishimaru *et al.* [16] Briefly, these authors demonstrated that, for scatterers that are small compared to the optical wavelength, the diffusion theory gives good agreement with experimental data. For scatterers that are large compared to the wavelength, the diffusion theory is applicable only when the optical absorption depth is large compared to the scattering distance ($\geqslant 20$). Finally, if the scatterer is a strong absorber [$\mu_a/(\mu_a+\mu_s) \geqslant 10^{-2}$, or $\mu_s/\mu_a \ll 100$] the diffusion theory may not be valid.

Within the framework of the diffusion approximation of the radiative transfer theory, a number of analytical approaches have been considered. Boas and Yodh [17] have developed a diffusion correlation formalism to characterize dynamical and optical spatial inhomogeneities in turbid me-

dia. Farrell, Patterson, and Wilson [18] have considered the steady-state diffuse-photon-density field in a semi-infinite turbid medium under continuous (dc) optical excitation. They developed a three-dimensional theory of the spatial profile of diffuse reflectance in the medium, using a Green-function approach. The exact boundary condition in this case is that, at the interface between the turbid medium and its (nondiffuse) surroundings, there should be no diffuse intensity entering the medium from outside (Ref. [14], Chap. 9.2). Furthermore, the diffuse source is extended, distributed in space inside the turbid medium. In order to be able to use the Green-function formalism, Farrell, Patterson, and Wilson [18] replaced the extended source with a single isotropic point source located at a depth equal to the scattering mean-free path. They also forced the photon fluence rate to zero at a position outside the actual interface (''extrapolated boundary'') equal to $z_b=2AD$, where A is a constant related to the internal reflection [see Sec. II; Eq. (11)] and D is the diffusion constant. In this manner the Green function satisfies homogeneous Dirichlet boundary conditions, but the diffusion equation is not accurate outside the physical boundaries of the turbid medium [19]. The same approach regarding boundary conditions was adopted by Patterson [20] in his treatment of the frequency dependence of the harmonic oscillation of a diffuse-photon-density wave (DPDW) in a turbid medium. Farrell, Patterson, and Wilson [18] further compared their Green-function-based diffuse-radial-reflectance model to Monte Carlo simulations of the semi-infinite turbid medium. They found some anomalies in their photon diffusion model, notably that the diffusion theory breaks down when the equivalent point-scatterer source is ''too close'' to the surface of the turbid medium. They also noticed that the single scatterer source gives better agreement with Monte Carlo simulation at short distances from the surface than the physically more realistic extended scattering source, a fact they called ''counterintuitive.'' The boundary conditions for the diffusion approximation are nontrivial, because near the boundaries of a turbid medium this approximation breaks down as the distance to the boundary becomes on the order of a photon mean-free path. In this spatial regime diffusive transport crosses over to free propagation (balistic photons). Much theoretical consideration has been given to this so-called ''skin layer'' [21,22]. It is clear that the nature of the approximation used to replace the exact photon source and boundary conditions at the turbid medium-air interface is a major unresolved issue in any analytical model of diffuse photon propagation in this system, especially at, or near, the interface, which is the main probe region of back-scattered-mode FD-PTR detection.

In this paper a theoretical formalism of FD-PTR in turbid media is developed, using exact boundary conditions consistent with the diffusion approximation of the radiative transfer theory. The theory develops and uses a three-dimensional model of the DPDW field as the modulated thermal-wave source in a turbid medium of finite thickness. Simulations of the DPDW and the thermal-wave fields generated by the diffuse optical volume distributions are also given to demonstrate the physical characteristics of the technique.

II. DIFFUSE-PHOTON-DENSITY-WAVE BOUNDARY VALUE PROBLEM

Laser fluence (or irradiance) in a turbid medium can be expressed as the superposition of coherent and diffuse components. The relative intensities depend on how scattering the medium is. For highly scattering media the diffuse component is almost isotropic, which allows the photon-density field to be expressed in a series of Legendre functions [16], leading to spherical harmonics [23]. The time-dependent photon density can be derived from the radiative transfer equation upon substitution of the first (isotropic) term in the foregoing series expansion,

$$D\nabla^2\rho_d(r,t)-\frac{1}{\upsilon}\frac{\partial}{\partial t}\rho_d(r,t)-\mu_a\rho_d(r,t)=-S(r,t), \quad (1)$$

where υ is the speed of light in the turbid medium, D is the optical diffusion coefficient, and $S(r,t)$ is the optical source function. For a harmonic optical source of cylindrical symmetry, such as an amplitude-modulated Gaussian laser beam at angular frequency ω, the temporal Fourier transform of Eq. (1) yields the DPDW (or *diffuse radiant energy fluence rate* field [23]), $\psi_d[\mathrm{Wm}^{-2}]$, equation [24] in cylindrical coordinates $\mathbf{r}=(r,\theta,z)$,

$$\nabla^2\psi_d(\mathbf{r},\omega)-\sigma_p^2(\omega)\psi_d(\mathbf{r},\omega)=-3\mu_s(\mu_t+g\mu_a)\times I(r,\omega)e^{-\mu_t z}. \quad (2)$$

Here a source strength depth distribution was assumed that decreases exponentially into the turbid medium (Bouguet's law) with total attenuation (extinction) coefficient

$$\mu_t=\mu_a+\mu_s \quad [\mathrm{m}^{-1}], \quad (3)$$

$\sigma_\rho(\omega)$ is the complex diffuse photon-density wave number, defined in Eq. (7). $I(r,\omega)$ is the radial fluence distribution (Wm^{-2}) of the photon source. g is the mean cosine of the scattering function $p(\theta)$ of the photon over all spatial directions described by the solid angle Ω; it can be thought of as an asymmetry parameter for anisotropic multiple scattering [25]. It can be defined as

$$g=\frac{\int_{4\pi}p(\theta)\cos\theta\, d\Omega}{\int_{4\pi}p(\theta)d\Omega}. \quad (4)$$

Mean cosine values range over the interval $-1\leqslant g\leqslant 1$. $g=0$ indicates balanced forward and backward scattering (e.g., isotropic or Rayleigh scattering), where $p(\theta)$ is constant (and equal to the single-scattering albedo $W_o=\mu_s/\mu_t$) [23]. Negative values of g are associated with net backward scattering, while positive values of g indicate net forward scattering. $g=1$ implies entirely forward scattering, where $p(\theta)$ is proportional to the Dirac delta function in the forward direction, $\theta=0$. It should be noted that the albedo W_o refers to a single photon and is generally different from the

transport albedo $a' = \mu_s'/(\mu_a + \mu_s')$ introduced by Eason *et al.* [26] and used in the Green-function formalism by Farrell, Patterson, and Wilson [18] a' is a collective photon property resulting from spatial summation of scattered photons (e.g., by an integrating sphere in total diffuse reflectance measurements). Also

$$\mu_s' \equiv (1-g)\mu_s \quad (\mathrm{m}^{-1}), \tag{5}$$

is the transport (or reduced) scattering coefficient. μ_s' becomes equal to μ_s only in the limiting case of fully isotropic scattering. It must be further noted that there is no contradiction between the range of validity of the time-dependent photon diffusion equation (1) and the possibility for nonisotropic photon distribution in the turbid medium as expressed by the definition of the mean cosine g, Eq. (4): The ''almost isotropic'' assumption underlying Eq. (1) and its Fourier transform, Eq. (2), represent an approximation in the limiting case where multiple scattering is dominant, regardless of its spatial distribution. For this reason, Ishimaru *et al.* [16] warn that near the surface of a turbid medium the diffusion solution may not be applicable. We will return to this point in the development of the FD-PTR theory in turbid media, Sec. V, on discussing the infrared radiometric probe, the depth averaging of which tends to reduce the effects of the inability of the diffusion approximation to describe the very near surface ballistic photon region. In view of the almost entirely forward scattering of photons in tissue, g values range between [27] 0.6 and 0.98. Therefore, the foregoing remarks regarding the consistency of the diffusion formalism are quite relevant.

Returning to the DPDW equation (2), the radial distribution of the Gaussian optical source at the surface of the turbid medium can be described as

$$I(r,\omega) = \frac{P(1-R)}{2\pi W^2} e^{-2r^2/W^2}(1+e^{i\omega t}) \quad (\mathrm{W/m}^2), \tag{6}$$

where P is the incident laser power, R is the total outward interfacial reflectance, which controls the amount of radiation that enters the turbid medium. R is distinct from the diffuse reflectance, which is generated following photon interactions with the medium. W is the laser-beam spotsize. The complex diffuse-photon wave number is defined as [24]

$$\sigma_\rho(\omega) = \sqrt{\frac{1-i\omega\tau_a}{D_{\mathrm{eff}}\tau_a}} \quad (\mathrm{m}^{-1}). \tag{7}$$

This definition is convenient, as it introduces the concepts of a diffuse-photon lifetime, $\tau_a \equiv (v\mu_a)^{-1}$, a function of the optical absorption properties of the medium; and of the effective photon diffusivity

$$D_{\mathrm{eff}} \equiv vD = \frac{v}{3[\mu_a + (1-g)\mu_s]} \quad (\mathrm{m}^2/\mathrm{s}). \tag{8}$$

The exact boundary condition at each interface is the requirement that there should be no diffuse intensity entering the turbid medium from outside (Ref. [14], Sec. 9-2). Applying this condition to the case of a turbid layer of finite thickness L and normal laser incidence, yields the boundary conditions on the isotropic DPDW field function (also known as fluence rate [18]), Ψ_d

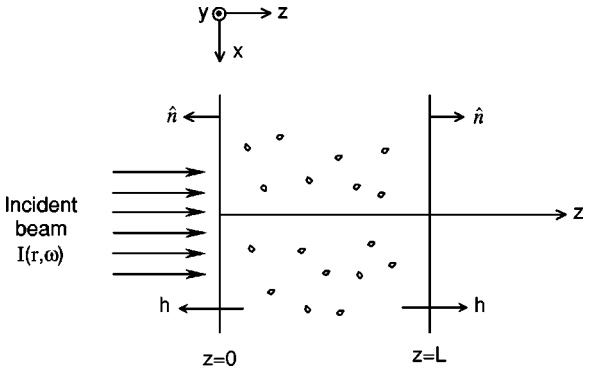

FIG. 1. Cross-sectional geometry of a slab of turbid matter of thickness L, optically excited by a harmonically modulated Gaussian laser beam of spotsize W, modulation frequency $f = \omega/2\pi$ and fluence given by Eq. (6).

$$\psi_d(r,0;\omega) - A\frac{\partial}{\partial z}\psi_d(r,z;\omega)\big|_{z=0} = -3\mu_s g A I(r,\omega), \tag{9}$$

and

$$\psi_d(r,L;\omega) + A\frac{\partial}{\partial z}\psi_d(r,z;\omega)\big|_{z=L} = 3\mu_s g A I(r,\omega)e^{-\mu_t L}. \tag{10}$$

Here the constant A is given as follows [14,18,28]

$$A = 2D\left(\frac{1+r_{21}}{1-r_{21}}\right) \equiv 2D\xi \quad (\mathrm{m}). \tag{11}$$

r_{12} is the internal reflectance, defined as the ratio of the upward-to-downward hemispherical diffuse optical fluxes at the boundary [28]. This definition of A (in the normalized form $A \to A/2D$) has been used by Groenhuis, Ferwerda, and Bosch [29] in the steady-state limit of Eq. (1): $\partial\rho_d(\mathbf{r},t)/\partial t = 0$; $\rho_d(\mathbf{r},t) = \psi_d(\mathbf{r},\infty) \equiv \psi_d(\mathbf{r})$, along with an empirical relationship between r_{21} and the relative refractive index n_{21}. The boundary conditions (9), (10), albeit derived from exact photon conservation considerations across the diffuse/ambient interface with rigorous mathematical manipulations, are approximate to the extent that the diffusion equation (2) itself holds only for the region far from the boundary and the source [16]. Nevertheless, in keeping with the phenomenological character of the diffusion approximation, these boundary conditions are optimal, since they are consistent with optical energy conservation principles at the turbid medium interfaces, Fig. 1. To compare with the Green-function approximation [18], the boundary condition (9) in a scattering medium readily reduces to the boundary-mismatched homogeneous condition [30]

$$\psi_d(r) - A\frac{\partial}{\partial z}\psi_d(r) = 0, \tag{12}$$

only if $g=0$ (purely isotropic scattering). Therefore, it can be concluded that the present approach removes the internally inconsistent use of the homogeneous boundary condition (12) with highly forward scattered photons in tissue [27], where $g\sim 1$. That inconsistency, nevertheless, is internal to the Green-function formalism and only impacts the calculated values of μ_s through the measured values of μ_s', Eq. (5), because g never appears independently of μ_s' in that formalism [18].

III. DIFFUSE AND COHERENT PHOTON-DENSITY-WAVE FIELDS

First, we turn to the problem of the DPDW field. The DPDW boundary-value problem of Eqs. (2), (9), and (10) can be solved analytically in cylindrical coordinates for Gaussian laser beam excitation of the type of Eq. (6), using the Hankel transformation. The cross-sectional geometry of a slab of turbid matter is shown in Fig. 1. It is convenient to define the total interaction coefficient

$$\mu_t' \equiv \mu_t - g\mu_s = \mu_a + (1-g)\mu_s = \mu_a + \mu_s' \quad (\mathrm{m}^{-1}), \tag{13}$$

where the total attenuation coefficient μ_t is given in Eq. (3). Equation (2) can be written

$$\nabla^2\psi_d(r,z;\omega) - \sigma_p^2\psi_d(r,z;\omega) = -\frac{1}{D}G(r,z;\omega), \tag{14a}$$

where

$$G(r,z;\omega) \equiv C_1(\omega)e^{-2r^2/W^2 - \mu_t z}, \tag{14b}$$

$$D = 1/3\mu_t', \tag{14c}$$

and

$$C_1(\omega) \equiv \frac{(1-R)P\mu_s}{2\pi W^2}\left(\frac{\mu_t + g\mu_a}{\mu_t - g\mu_s}\right)(1+e^{i\omega t}). \tag{14d}$$

By virtue of the circular symmetry of the laser excitation beam, it is convenient to take the Hankel transform of $\psi_d(r,z;\omega)$,

$$\tilde{\phi}_d(z;\lambda,\omega) = \int_0^\infty \psi_d(r,z;\omega)J_o(\lambda r)r\,dr, \tag{15}$$

where $J_o(x)$ is the Bessel function of the first kind of order zero. Equation (14a) is thus transformed to an ordinary differential equation

$$\frac{d^2}{dz^2}\tilde{\phi}_d(z;\lambda,\omega) - \beta^2\tilde{\phi}_d(z;\lambda,\omega) = -\frac{1}{D}\tilde{G}(z;\lambda,\omega), \tag{16a}$$

with

$$\beta^2(\lambda,\omega) \equiv \lambda^2 + \sigma_p^2(\omega) \quad (\mathrm{m}^{-2}), \tag{16b}$$

and

$$\tilde{G}(z;\lambda,\omega) \equiv C_2(\omega)e^{-(\lambda^2W^2)/8 - \mu_t z}(1+e^{i\omega t}), \tag{16c}$$

$$C_2(\omega) = W^2C_1(\omega). \tag{16d}$$

For arbitrary radial source distributions $I(r,\omega)$, the Hankel transform $\tilde{G}$ may be generalized,

$$\tilde{G}(z;\lambda,\omega) = \left(\frac{\mu_t + g\mu_a}{\mu_t - g\mu_s}\right)\mu_s e^{-\mu_t z}\tilde{I}(\lambda,\omega). \tag{17}$$

The boundary conditions (9)–(10) transform to

$$\tilde{\phi}_d(0;\lambda,\omega) - A\frac{d}{dz}\tilde{\phi}_d(z;\lambda,\omega)\big|_{z=0} = -3\mu_s gA\tilde{I}(\lambda,\omega), \tag{18a}$$

$$\tilde{\phi}_d(L;\lambda,\omega) + A\frac{d}{dz}\tilde{\phi}_d(z;\lambda,\omega)\big|_{z=0} = 3\mu_s gAe^{-\mu_t L}\tilde{I}(\lambda,\omega). \tag{18b}$$

The solution to the Hankel-transformed boundary-value problem is tedious but straightforward,

$$\tilde{\phi}_d(z;\lambda,\omega) = A_1e^{\beta z} + A_2e^{-\beta z} - \frac{\tilde{G}(z;\lambda,\omega)}{D(\mu_t^2 - \beta^2)}, \tag{19}$$

where

$$A_1 = \frac{F_2(1+A\beta) - F_1(1-A\beta)}{(1+A\beta)^2e^{\beta L} - (1-A\beta)^2e^{-\beta L}}, \tag{20a}$$

and

$$A_2 = \frac{F_1(1+A\beta)e^{\beta L} - F_2(1-A\beta)}{(1+A\beta)^2e^{\beta L} - (1-A\beta)^2e^{-\beta L}}, \tag{20b}$$

with

$$F_1 = \left[\frac{1}{D}\left(\frac{1+\mu_t A}{\mu_t^2 - \beta^2}\right)\left(\frac{\mu_t + g\mu_a}{\mu_t - g\mu_s}\right) - \frac{2g}{\mu_t'}\right]\mu_s\tilde{I}(\lambda,\omega), \tag{21a}$$

and

$$F_2 = \left[\frac{1}{D}\left(\frac{1-\mu_t A}{\mu_t^2 - \beta^2}\right)\left(\frac{\mu_t + g\mu_a}{\mu_t - g\mu_s}\right) + \frac{2g}{\mu_t'}\right]\mu_s e^{-\mu_t L}\tilde{I}(\lambda,\omega). \tag{21b}$$

For the Gaussian laser beam considered in this work,

$$\tilde{I}(\lambda,\omega)=\frac{P(1-R)}{2\pi W^2}e^{i\omega t}\int_0^\infty e^{-2r^2/W^2}J_o(\lambda r)r\,dr$$

$$=\frac{P(1-R)}{2\pi}e^{-(\lambda^2W^2/8)+i\omega t}. \quad (22)$$

For simplicity, only the oscillating component of the modulated incident laser fluence Eq. (6) is considered in the calculations, and the time-varying exponential $e^{i\omega t}$ is usually omitted. The dc component is of no experimental interest, as its demodulated contribution (e.g., by a phase-sensitive lock-in analyzer) is zero.

To complete the solution, the coherent photon-density wave must be added to the diffuse-photon-density distribution:

$$\psi_t(r,z;\omega)=\psi_c(r,z;\omega)+\psi_d(r,z;\omega). \quad (23)$$

Here the oscillatory coherent field source can be easily obtained by modification of the dc source [16] as follows:

$$\psi_c(r,z;\omega)=\frac{P(1-R)}{2\pi W^2}e^{-2(r^2/W^2)-\mu_t z+i\omega t}. \quad (24)$$

For arbitrary optical-source distributions, the Hankel transform of ψ_c is

$$\tilde{\phi}_c(z;\lambda,\omega)=\tilde{I}(\lambda,\omega)e^{-\mu_t z+i\omega t}. \quad (25)$$

Combining this term with Eq. (19) and rearranging yields the Hankel transform of the total photon-density-wave field in the turbid medium of Fig. 1.

$$\tilde{\phi}_t(z;\lambda,\omega)=\tilde{\phi}_c(z;\lambda,\omega)+\tilde{\phi}_d(z;\lambda,\omega)$$

$$=\frac{(F_1-\gamma F_2e^{-\beta L})e^{-\beta L}+(F_2-\gamma F_1e^{-\beta L})e^{-\beta(L-z)}}{(1+A\beta)(1-\gamma^2e^{-2\beta L})}+\left[1-\frac{1}{D}\left(\frac{\mu_t+g\mu_a}{\mu_t-g\mu_s}\right)\left(\frac{\mu_s}{\mu_t^2-\beta^2}\right)\right]e^{-\mu_t z}\tilde{I}(\lambda,\omega). \quad (26)$$

In this expression the interfacial diffuse-photon transfer coefficient γ has been defined as

$$\gamma\equiv\frac{1-A\beta}{1+A\beta}. \quad (27)$$

In the absence of scattering particles in the medium, we set $\mu_s=0$. This reduces $F_1=F_2=0$ in Eqs. (21a, 21b) and $\mu_t=\rho_\alpha$ in Eq. (3). The resulting Hankel transform of the photon-density-wave field, Eq. (26), reduces to

$$\tilde{\phi}_t(z;\lambda,\omega)=\tilde{I}(\lambda,\omega)e^{-\mu_a z}. \quad (28)$$

For a Gaussian source as in Eq. (22), Eq. (28) may be inverse transformed immediately, yielding the expected result

$$\psi_t(r,z;\omega)=\frac{P(1-R)}{2\pi W^2}e^{-2(r^2/W^2)-\mu_a z+i\omega t}. \quad (29)$$

IV. THE THERMAL-WAVE FIELD

The thermal-wave source in the turbid medium is generated through absorption and optical-to-thermal energy conversion of the total (diffuse+coherent) photon field, which is present in the medium as a result of laser excitation. Therefore, if $R_L(r,z;\omega)$ represents the volume loss rate of photons at depth z, then

$$R_L(r,z;\omega)=P_LN(r,z;\omega)\quad(\mathrm{m^{-3}\,s^{-1}}), \quad (30)$$

where P_L is the probability of single-photon loss per unit depth and $N(r,z;\omega)$ is the photon fluence (photons/m^{2}s) at the coordinate point $\mathbf{r}=(r,z)$. In a turbid medium with no intersystem crossing or photochemical photon conversion, $P_L=P_a+P_s$ (a: absorption, s: scattering). Therefore, for the creation of a thermal-wave source $Q(r,z;\omega)$ one writes

$$Q(r,z;\omega)=\varepsilon_\nu R_L^{\mathrm{NR}}(r,z;\omega)\quad(\mathrm{Wm^{-3}}), \quad (31)$$

where ε_ν $(=h\nu)$ is the energy of the (assumed monochromatic) photon emitted at frequency ν, and R_L^{NR} is the fraction of the photon loss-rate undergoing nonradiative transitions and thus being converted into heat. From Eqs. (30) and (31)

$$Q(r,z;\omega)=\varepsilon_\nu P_L^{\mathrm{NR}}N(r,z;\omega)=\varepsilon_\nu\eta_{\mathrm{NR}}\mu_aN(r,z;\omega), \quad (32)$$

where, $P_L^{\mathrm{NR}}=\mu_a\eta_{\mathrm{NR}}$ is the probability of an *absorbed* photon being converted into heat, as opposed to being scattered or consumed to generate luminescence, further excited-state creation, etc. Here η_{NR} is the nonradiative quantum efficiency. Since $\varepsilon_\nu N(r,z;\omega)=\psi_t(r,z;\omega)$, it follows that

$$Q(r,z;\omega)=\eta_{\mathrm{NR}}\mu_a\psi_t(r,z;\omega), \quad (33)$$

where $\psi_t(r,z;\omega)$ is the optical source function (energy fluence rate [18], in Wm^{-2}). In the case of a homogeneous nonscattering medium with radially uniform excitation source, Eq. (33) reduces to

$$Q(z;\omega)=\eta_{\mathrm{NR}}\mu_a\psi_{t0}(\omega)e^{-\mu_a z}=-\eta_{\mathrm{NR}}\frac{d}{dz}\psi_t(z,\omega), \quad (34)$$

where the Beer-Lambert absorption law was assumed $\psi_t(z,\omega)=\psi_{t0}(\omega)e^{-\mu_a z}$. For non-Beer-Lambert media, the

thermal source equation (33) must be used instead of taking the normal derivative of the optical source function.

For an arbitrary harmonic optical source, which creates the total photon-density-wave field $\psi_t(r,z;\omega)$, Eq. (23), in the turbid medium, the thermal-wave field is given by [24]

$$\nabla^2 T(r,z;\omega) - \sigma_t^2(\omega) T(r,z;\omega) = -\eta_{\mathrm{NR}}(\mu_a/k_t)\psi_t(r,z;\omega), \tag{35}$$

where

$$\sigma_t(\omega) = \sqrt{i\omega/D_t} \quad (\mathrm{m}^{-1}), \tag{36}$$

is the thermal wave number, D_t is the thermal diffusivity ($\mathrm{m}^2\mathrm{s}^{-1}$) and k_t is the thermal conductivity ($\mathrm{Wm}^{-1}\,\mathrm{K}^{-1}$) of the medium. In the geometry of Fig. 1 we assume homogeneous boundary conditions of the third kind [24]:

$$-k_t \hat{\mathbf{n}}\cdot\nabla T(r,z;\omega)\big|_{z=0,L} = hT(r,z;\omega)\big|_{z=0,L}. \tag{37}$$

Here $\hat{\mathbf{n}}$ is the outward unit vector normal to the surface at $z=0$, L, and h ($\mathrm{Wm}^{-2}\,\mathrm{K}^{-1}$) is the heat transfer coefficient. In the coordinate system of Fig. 1, $\hat{\mathbf{n}}\cdot\nabla = -\partial/\partial z\big|_{z=0}$ at $z=0$ and $\hat{\mathbf{n}}\cdot\nabla = \partial/\partial z\big|_{z=L}$ at $z=L$. The Hankel transform of the thermal-wave field

$$\tilde{\tau}(z;\lambda,\omega) = \int_0^\infty T(r,z;\omega) J_0(\lambda r) r\, dr, \tag{38}$$

is the solution to the ordinary boundary-value problem

$$\frac{d^2}{dz^2}\tilde{\tau}(z;\lambda,\omega) - q^2\tilde{\tau}(z;\lambda,\omega) = -\eta_{\mathrm{NR}}(\mu_a/k_t)\tilde{\phi}_t(z;\lambda,\omega), \tag{39}$$

$$-k_t\frac{d}{dz}\tilde{\tau}(z;\lambda,\omega)\big|_{z=0} = h\tilde{\tau}(0;\lambda,\omega), \tag{40a}$$

$$k_t\frac{d}{dz}\tilde{\tau}(z;\lambda,\omega)\big|_{z=L} = h\tilde{\tau}(L;\lambda,\omega). \tag{40b}$$

Here $\tilde{\phi}_t(z;\lambda,\omega)$ is given by the Hankel transform of the total-photon-density field, Eq. (26), and

$$q^2(\lambda,\omega) \equiv \lambda^2 + \sigma_t^2(\omega) \quad (\mathrm{m}^{-2}). \tag{40c}$$

From the structure of Eq. (26) and by inspection, the solution of Eq. (39) can be written in the form

$$\tilde{\tau}(z;\lambda,\omega) = B_1 e^{-\beta z} + B_2 e^{\beta z} + B_3 e^{-\mu_t z} + B_4 e^{qz} + B_5 e^{-qz}. \tag{41}$$

After a tedious but straightforward series of manipulations, the Hankel transform of the thermal-wave field can be written as

$$\begin{aligned}\tilde{\tau}(z;\lambda,\omega) = {} & B_1\left\{e^{-\beta t} + \left(\frac{k_t\beta - h}{1-e^{-2qL}}\right)\left(\frac{1}{h+k_tq}[e^{-(\beta+q)L} - e^{-2qL}]e^{qz} + \frac{1}{h-k_tq}[1-e^{-(\beta+q)L}]e^{-qz}\right)\right\} \\ & + B_2\left\{e^{\beta t} - \left(\frac{k_t\beta + h}{1-e^{-2qL}}\right)\left(\frac{1}{h+k_tq}[e^{-(q-\beta)L} - e^{-2qL}]e^{qz} + \frac{1}{h-k_tq}[1-e^{-(q-\beta)L}]e^{-qz}\right)\right\} \\ & + B_3\left\{e^{-\mu_t z} + \left(\frac{k_t\mu_t - h}{1-e^{-2qL}}\right)\left(\frac{1}{h+k_tq}[e^{-(\mu_t+q)L} - e^{-2qL}]e^{qz} + \frac{1}{h-k_tq}[1-e^{-(\mu_t+q)L}]e^{-qz}\right)\right\},\end{aligned} \tag{42}$$

with the following definitions:

$$B_1(\lambda,\omega) = \frac{\eta_{\mathrm{NR}}\mu_a}{k_t(\beta^2 - q^2)} b_1(\lambda,\omega), \tag{43a}$$

$$B_2(\lambda,\omega) = -\frac{\eta_{\mathrm{NR}}\mu_a}{k_1(\beta^2 - q^2)} b_2(\lambda,\omega), \tag{43b}$$

and

$$B_3(\lambda,\omega) = -\frac{\eta_{\mathrm{NR}}\mu_a}{k_t(\mu_t^2 - q^2)} b_3(\lambda,\omega), \tag{43c}$$

where, for an arbitrary optical-source radial distribution $I(r,\omega)$ with Hankel transform $\tilde{I}(\lambda,\omega)$,

$$b_1(\lambda,\omega) \equiv \frac{1}{H(\lambda,\omega)}(-F_1 + \gamma F_2 e^{-\beta L}), \tag{44a}$$

$$b_2(\lambda,\omega) \equiv \frac{1}{H(\lambda,\omega)}(F_2 - \gamma F_1 e^{-\beta L})e^{-\beta L}, \tag{44b}$$

$$b_3(\lambda,\omega) \equiv \left[1 - \frac{\mu_s}{D(\mu_t^2 - \beta^2)}\left(\frac{\mu_t + g\mu_a}{\mu_t - g\mu_s}\right)\right]\tilde{I}(\lambda,\omega), \tag{44c}$$

and

$$H(\lambda,\omega) \equiv (1 + A\beta)(1 - \gamma^2 e^{-2\beta L}). \tag{44d}$$

In the case of a TEM_{00} Gaussian laser beam, $\tilde{I}(\lambda,\omega)$ is given by Eq. (22). F_1 and F_2 are defined in Eq. (21); γ is defined in Eq. (27). Depending on the value of h, the two limiting cases of Eq. (42) for $h=0$ (adiabatic boundaries) and $h \to \infty$ (diathermal or isothermal boundaries) are obtained immediately.

V. THE FREQUENCY-DOMAIN PTR SIGNAL

Taking advantage of the cylindrical symmetry of the exciting Gaussian laser beam, we use the Hankel transformation for the thermal-wave field, Eq. (38). The Hankel transform of the PTR signal $U(r,\omega)$ can then be written as

$$\tilde{u}(\lambda,\omega)=C\int_{\Lambda_1}^{\Lambda_2}W(\Lambda)\mu_{\mathrm{IR}}(\Lambda)d\Lambda\int_0^L\tilde{\tau}(z;\lambda,\omega)e^{-\mu_{\mathrm{IR}}(\Lambda)z}dz, \tag{45}$$

where Λ denotes wavelength; Λ_1 and Λ_2 are the limits of the spectral bandwidth of the infrared detector; $W(\Lambda)$ is a wavelength-dependent coefficient involving the Planck distribution function and the spectral response of the detector [31]. C is a constant involving both instrumental factors (e.g., the infrared radiometric system transfer function), and the grouping of physical terms $4\sigma\varepsilon T_o^3$ for small thermal-wave amplitudes $|T_{\max}|\ll T_o$. T_o is the ambient temperature, σ is the Stefan-Boltzmann constant ($\sigma=5.6703\times10^{-8}\,\mathrm{W/m^2\,K^4}$) and ε is the emissivity of the turbid medium. The spectrally averaged Hankel transform $\langle\tilde{u}(\lambda,\omega)\rangle$ is given by

$$\langle\tilde{u}(\lambda,\omega)\rangle=\frac{\tilde{u}(\lambda,\omega)}{\int_{\Lambda_1}^{\Lambda_2}W(\Lambda)d\Lambda}. \tag{46}$$

Using the ''effective IR absorption/emission coefficient'' definition [32]

$$\langle\mu_{\mathrm{IR}}e^{-\mu_{\mathrm{IR}}z}\rangle=\frac{\int_{\Lambda_1}^{\Lambda_2}W(\Lambda)\mu_{\mathrm{IR}}(\Lambda)e^{-\mu_{\mathrm{IR}}(\Lambda)z}d\Lambda}{\int_{\Lambda_1}^{\Lambda_2}W(\Lambda)d\Lambda}, \tag{47}$$

we may write

$$\langle\tilde{u}(\lambda,\omega)\rangle=C\int_0^L\langle\mu_{\mathrm{IR}}e^{-\mu_{\mathrm{IR}}z}\rangle\tilde{\tau}(z;\lambda,\omega)dz$$

$$\simeq C\bar{\mu}_{\mathrm{IR}}\int_0^L\tilde{\tau}(z;\lambda,\omega)e^{-\bar{\mu}_{\mathrm{IR}}z}dz. \tag{48}$$

Here $\bar{\mu}_{\mathrm{IR}}$ is the effective IR absorption coefficient of the medium. Note that the spectrally averaging notation $\langle\cdots\rangle$ was dropped from the second (approximate) version of Eq. (48) and was replaced by an overbar, to indicate spatial averaging over the depth coordinate z, in agreement with accepted practice in the analysis of photothermal radiometric signals [33]. Majaron *et al.* [32] have shown that $\bar{\mu}_{\mathrm{IR}}$ may depend strongly on probed depth z. Simulations using a correction algorithm for pulsed-laser PTR of some biomedical materials demonstrated that errors up to 30% of the signal value may occur by assuming constant $\bar{\mu}_{\mathrm{IR}}$. Nevertheless, in FD-PTR of turbid media, relatively large values of $\bar{\mu}_{\mathrm{IR}}$ are obtained [11,20,23], indicating IR absorption/emission depths on the order of 5–33 μm. Within this shallow depth range, an essentially surface localization of the IR emission contribution is expected, compared with the much longer absorption length, $1/\mu_a$, of the laser exciting radiation. Furthermore, it has been shown [32] that the spectral variation of $\mu_{\mathrm{IR}}(\Lambda)$ can be much reduced at shallow depths, and thus the error committed using the approximate Eq. (48) may be much less than 30%. This would be the case of scattering media with $\mu_s\gg\mu_a$, a condition typically valid in turbid tissue environment [2,23]. Computationally, an effective value of $\bar{\mu}_{\mathrm{IR}}$ can be extracted over all probed depths from a multiparameter fit of the entire frequency-response curve (amplitude and phase) of the turbid medium. Using the approximate version of Eq. (48) for the Hankel transform $\langle\tilde{u}(\lambda,\omega)\rangle$ of the PTR signal, $U(r,\omega)$, we obtain the Hankel transform of the backscattered PTR signal

$$\begin{aligned}\langle\tilde{u}(\lambda,\omega)\rangle=C\bar{\mu}_{\mathrm{IR}}\times\Bigg[B_1\Bigg\{&\frac{1-e^{-(\beta+\bar{\mu}_{\mathrm{IR}})L}}{\beta+\tilde{\mu}_{\mathrm{IR}}}+\left(\frac{k_t\beta-h}{1-e^{-2qL}}\right)\left(\frac{1-e^{-(\bar{\mu}_{\mathrm{IR}}-q)L}}{(h+k_tq)(\bar{\mu}_{\mathrm{IR}}-q)}[e^{-(\beta+q)L}-e^{-2qL}]\right.\\&\left.+\frac{1-e^{-(\bar{\mu}_{\mathrm{IR}}+q)L}}{(h-k_tq)(\bar{\mu}_{\mathrm{IR}}+q)}[1-e^{-(\beta+q)L}]\right)\Bigg\}+B_2\Bigg\{\frac{1-e^{-(\bar{\mu}_{\mathrm{IR}}-\beta)L}}{\bar{\mu}_{\mathrm{IR}}-\beta}-\left(\frac{k_t\beta+h}{1-e^{-2qL}}\right)\left(\frac{1-e^{-(\bar{\mu}_{\mathrm{IR}}-q)L}}{(h+k_tq)(\bar{\mu}_{\mathrm{IR}}-q)}\right.\\&\times[e^{-(q-\beta)L}-e^{-2qL}]+\left.\frac{1-e^{-(\bar{\mu}_{\mathrm{IR}}+q)L}}{(h-k_tq)(\bar{\mu}_{\mathrm{IR}}+q)}[1-e^{-(q-\beta)L}]\right)\Bigg\}+B_3\Bigg\{\frac{1-e^{-(\bar{\mu}_{\mathrm{IR}}+\mu_t)L}}{\tilde{\mu}_{\mathrm{IR}}+\mu_t}+\left(\frac{k_t\mu_t-h}{1-e^{-2qL}}\right)\\&\times\left(\frac{1-e^{-(\bar{\mu}_{\mathrm{IR}}-q)L}}{(h+k_tq)(\bar{\mu}_{\mathrm{IR}}-q)}[e^{-(\mu_t+q)L}-e^{-2qL}]+\frac{1-e^{-(\bar{\mu}_{\mathrm{IR}}+q)L}}{(h-k_tq)(\bar{\mu}_{\mathrm{IR}}+q)}[1-e^{-(\mu_t+q)L}]\right)\Bigg\}\Bigg].\end{aligned} \tag{49}$$

The foregoing complicated function is the result of a depth integration as indicated by Eq. (48), which utilizes the DPDW field in the diffusion approximation. The contributions of the subsurface values of this field to the forcing function $\psi_t(r,z;\omega)$, Eq. (35), would tend to diminish the effects of the nonvalidity of the diffusion solution very near the surface [16]. The contributions of the surface and very near surface values of ψ_t in the integral (48) are expected to

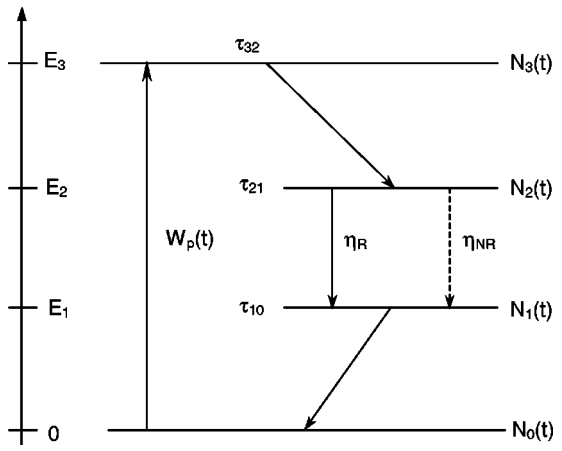

FIG. 2. Excited-state manifold of a generic four-level turbid fluorophore system.

decrease with decreasing $\overline{\mu}_{\mathrm{IR}}$, which would result in a higher-accuracy approximation of the PTR expression, the inverse Hankel transform of Eq. (49). Specifically, an improved degree of validity of the DPDW expression $\psi_t(\mathbf{r};\omega)$ as the forcing function of the thermal-wave PTR field is expected when the scattering mean-free-path in the turbid medium is short compared to $1/\overline{\mu}_{\mathrm{IR}}$. A detailed investigation of this issue, however, still remains a task for the future.

VI. EXCITED-STATE RELAXATION CONTRIBUTIONS TO THE FD-PTR SIGNAL

Several studies of turbid fluorophores with excited-state relaxation mechanisms have been reported within the Green-function formalism of the DPDW field [34–36]. In those studies fluorophores were treated as two-level quantum systems and excited-state optical saturation effects were ignored. Most importantly, when detection is effected via photothermal mechanisms such as PTR, the possibility of saturation, as well as the nonradiative quantum yield, η_{NR}, must be taken into account as they both induce optical-to-thermal energy conversion [37]. Owing to the frequent occurrence of this situation in laser-excited turbid media [2,14,34–36], a complete thermal-wave theory of nonradiatively relaxing diffuse photon-density waves must allow for excited-state relaxations of fluorophores.

Figure 2 shows a generic four-level turbid fluorophore system, in which level $|2\rangle$ relaxes both radiatively (producing fluorescence) and nonradiatively (producing heat). Assuming an optical pumping rate $W_p(t)=\frac{1}{2}W_{po}(1+e^{i\omega t})$ to the upper state $|3\rangle$, from the ground state $|0\rangle$, the following rate equations hold:

$$\frac{d}{dt}N_3(t)=W_p(t)N_o(t)-\frac{N_3(t)}{\tau_{32}}, \tag{50a}$$

$$\frac{d}{dt}N_2(t)=\frac{N_3(t)}{\tau_{32}}-\frac{N_2(t)}{\tau_{21}}, \tag{50b}$$

$$\frac{d}{dt}N_1(t)=\frac{N_2(t)}{\tau_{21}}-\frac{N_1(t)}{\tau_{10}}, \tag{50c}$$

and

$$\frac{d}{dt}N_o(t)=-W_p(t)N_o(t)+\frac{N_1(t)}{\tau_{10}}. \tag{50d}$$

Making the reasonable assumptions that τ_{32}, $\tau_{10}\ll\tau_{21}$, Eqs. (50) yield

$$N_3(t)\approx\tau_{32}W_p(t)N_o(t)\approx 0, \tag{51a}$$

$$\frac{d}{dt}N_2(t)\approx W_P(t)N_o(t)-\frac{N_2(t)}{\tau_{21}}, \tag{51b}$$

$$\frac{d}{dt}N_1(t)\approx 0\Rightarrow N_1(t)\approx(\tau_{10}/\tau_{21})N_2(t)\approx 0. \tag{51c}$$

Therefore, the only comparatively populated levels are $|0\rangle$ and $|2\rangle$. For level $|2\rangle$.

$$\frac{d}{dt}N_2(t)\approx W_P(t)[N_T-N_2(t)]-\frac{N_2(t)}{\tau_{21}}, \tag{52a}$$

or, in terms of a kinetic equation for $N_2(t)$,

$$\frac{d}{dt}N_2(t)+[W_P(t)+\tau_{21}^{-1}]N_2(t)\approx W_P(t)N_T, \tag{52b}$$

where, N_T is the total particle density in the fluorophore (a constant): $N_T=\Sigma_{j=0}^{3}N_j(t)$. Letting the modulated density of fluorophore in level $|2\rangle$ be described as $N_2(t)=\frac{1}{2}N_{20}(1+e^{i\omega t})$, using Eq. (52b), and separating out the $e^{i\omega t}$ terms from dc and second-harmonic contributions, consistently with synchronous lock-in detection, we obtain

$$N_{20}(\omega)=\frac{W_{po}\tau_{21}N_T}{1+W_{po}\tau_{21}+i\omega\tau_{21}}. \tag{53}$$

This expression for the modulated particle density in level $|2\rangle$ does include optical saturation effects, which depend on the value of the pumping-rate magnitude W_{po}, via the dependence of the optical absorption coefficient on this quantity.

The thermal-wave source at the fundamental frequency $f=\omega/2\pi$ is given by the total heat production rate, as a sum over all nonradiative decay pathways from all levels,

$$\dot{q}(t)\approx W_p(t)E_{32}N_T+\left[\frac{1}{\tau_{21}}(\eta_{\mathrm{NR}}E_{21}+E_{10})-W_p(t)E_{32}\right]N_2(t)\quad(\mathrm{Wm}^{-3}). \tag{54}$$

Here the nonradiative quantum efficiencies of levels $|3\rangle$ and $|4\rangle$ were assumed to be equal to one (i.e., there is only one fluoresent level). Writing $\dot{q}(t)=\dot{Q}(\omega)(1+e^{i\omega t})$ and retaining only terms modulated by the factor $e^{i\omega t}$, we obtain

$$\dot{Q}(\omega)=\frac{1}{2}W_{po}E_{32}[N_T-N_{20}(\omega)]+\frac{1}{2}\left(\frac{\varepsilon_{\rm NR}}{\tau_{21}}\right)N_{20}(\omega), \tag{55}$$

where

$$\varepsilon_{\rm NR}=\eta_{\rm NR}E_{21}+E_{10}, \tag{56}$$

is the total excited-state energy from levels $|2\rangle$ and $|1\rangle$ released nonradiatively with delay time τ_{21}. The fraction of the *total* input energy to the turbid medium that is released nonradiatively and thus creates a thermal-wave source in the medium is determined from

$$W_p(t)E_{30}N_T=\mu_a^{(30)}I(t), \tag{57}$$

where, $I(t)=\frac{1}{2}I_o(1+e^{i\omega t})$ is the incident laser fluence. $\mu_a^{(30)}$ is the absorption coefficient between levels $|0\rangle$ and $|3\rangle$. It follows that the optical pumping rate is

$$W_{po}=\frac{\mu_a^{(30)}I_o}{N_TE_{30}} \quad [\mathrm{s}^{-1}], \tag{58}$$

If, for simplicity, a three-level system is assumed, with $E_{32}=0$ in Fig. 2, then $E_{30}=E_{20}$, and Eqs. (53) and (55) yield the medium heating rate in terms of the amplitude W_{po},

$$\dot{Q}(\omega)=\frac{1}{2}\left(\frac{W_{po}\varepsilon_{\rm NR}N_T}{W_{po}\tau_{21}+1+i\omega\tau_{21}}\right). \tag{59}$$

Now, under intense pumping conditions $\tau_{21}\gg W_{po}^{-1}$, Eq. (59) reduces to $\dot{Q}(\omega)\approx\frac{1}{2}(\varepsilon_{\rm NR}/\tau_{21})N_T$. This result indicates that $N_{20}\approx N_T$, as expected from the intense ground-to-excited-state transition rate and the long lifetime of level $|2\rangle$.

Finally, Equations (58) and (59) are used to modify the thermal-wave source in Eq. (35) so as to take into account the nonzero excited-state relaxation rate, as follows:

$$\eta_{\rm NR}\mu_a\psi_t(r,z;\omega)\rightarrow\mu_a^{(20)}\psi_i^*(r,z;\omega), \tag{60}$$

where, $\mu_a^{(20)}$ denotes the optical absorption coefficient inducing the optical transition from level $|0\rangle$ to $|2\rangle$ in the simplified three-level fluorophore. $\psi_t^*(\mathbf{r};\omega)$ is identical in form to $\psi_t(\mathbf{r};\omega)$, with Hankel transform given by Eq. (26), but for the modified source distribution

$$I(r,\omega)\rightarrow\left(\frac{\varepsilon_{\rm NR}/E_{20}}{W_{po}\tau_{21}+1+i\omega\tau_{21}}\right)I(r,\omega), \tag{61}$$

where, for a Gaussian laser beam $I(\mathbf{r},\omega)$ is given as indicated in Eq. (22). If $E_{10}=0$ and $\tau_{21}=0$, then the term in parentheses is equal to $\eta_{\rm NR}$ of the single excited state, and the thermal source for zero fluorescence lifetime on the right-hand side (rhs) of Eq. (35) is obtained. If the rate $W_{po}\ll\tau_{21}^{-1}$ (weak optical pumping), then the usual phase lag $\theta=-\tan^{-1}(\omega\tau_{21})$ due to unsaturated excited-state relaxation is observed [34–36]. On the other hand, intense optical pumping such that $W_{po}\tau_{21}\gg1$ and $W_{po}\gg\omega$ must be taken into account in Eqs. (60) and (61) by recognizing, from Eqs. (58) and (59), that in a three-level fluorophore,

$$\mu_a^{(20)}I_o\approx W_{po}E_{20}N_T\Rightarrow\mu_a^{(20)}=\mu_{a\,\max}^{(20)}. \tag{62}$$

Therefore, multiplication of Eq. (61) with $\mu_a^{(20)}$ and use of Eq. (62) yields the result

$$\mu_a^{(20)}I(r,\omega)\rightarrow N_T\left(\frac{\varepsilon_{\rm NR}}{\tau_{21}}\right)\times(\text{spatial beam distribution}). \tag{63}$$

This limit is independent of the optical absorption coefficient, as expected from optically saturated transitions. In conclusion, the modified $I(r,\omega)$ as indicated in Eq. (61) must be inserted in the calculation of the thermal-wave source terms and their Hankel transforms in Eqs. (42)–(44), when three-level, relaxing fluorescent DPDW fields in turbid media are involved. The extension to more levels and excited-state manifolds is straightforward.

VII. COMPUTER SIMULATIONS

The following simulations of the theory are meant to represent the diffusion-photon wave and the associated thermal-wave behavior of soft tissue and light scattering emulsions, such as intralipid, with parameters [38–40]: μ_s in the range $\leqslant10^3\,\mathrm{mm}^{-1}$, μ_a in the range $\leqslant$ 0.01–10 mm^{-1}, and $A=2.75$–3.50. For these types of turbid media the diffusion approximation, Eq. (2) is valid for modulation frequencies $f<50$ GHz. While the photon field is probably not diffuse everywhere in such low-to-intermediate albedo tissues, the inclusion of the collimated (coherent) photon density, $\Psi_c(r,z;\omega)$, with its coefficients properly matched to the diffuse solution, provides a reasonable accuracy improvement for this troublesome intermediate albedo regime. This, in turn, improves the computational accuracy greatly. Several simulations of the theory were performed, first in terms of the total diffuse-photon field as represented by the numerical inverse Hankel transform of Eq. (26). Then the spatially distributed photon field was used as the source to the thermal-wave problem, and the temperature oscillation, i.e., the Hankel transform of Eq. (42) was calculated numerically. In some cases the actual infrared radiometric signal was generated as the numerical inverse transform of Eq. (49). The Hankel integral is an improper integral, i.e., its upper limit is infinite. It was verified that, based on the physical quantity represented by the complex integrand, the integral exists and approaches a finite value as the upper limit of integration approaches infinity. The integration was calculated using the improper integral routine, *qromo* [41,42] with *midpnt* taken from Ref. [41]. Due to the large number of parameters involved in the foregoing equations, a considerable number of simulations were performed. In what follows, the behavior of the various fields as a function of a given parameter will be described in some selected cases of experimental importance. All simulations assume TEM_{00} Gaussian laser beam profiles.

A. Dependence on modulation frequency and turbid-medium thickness

Simulations were performed versus optical intensity modulation frequency in the range 10 Hz–100 kHz, which is perti-

nent to frequency-domain PTR measurements. For the DPDW field, the value of the mean cosine was assumed to be $g=0.965$, i.e., that of scattering tissue phantoms [42], and was calculated independently using Mie theory [43]. The value range of $\xi\equiv(1+r_{21})/(1-r_{21})$ in Eq. (11) for turbid media is 5.0–9.5 [28]. In this work the value $\xi=3.517$ was used, corresponding to $r_{21}=0.557$, which was independently measured for tissue phantoms [42]. In one set of simulations with turbid slabs of various thicknesses, L, and infinite lateral dimensions and $\mu_a=0.1$ and $\mu_s=31.8\,\mathrm{mm}^{-1}$, Fig. 3(a), the $(r,z)=(0,0)$ coordinate DPDW phase lag increases with increasing frequency (although the absolute phase shift is on the order of $30-40\times10^{-6}$ degrees) and the amplitude remains flat up to 100 kHz. This behavior is consistent with experimental results obtained by Lacowitz and Berndt [44] in arm and finger tissue and by Patterson *et al.* for a scattering emulsion [45]. The phase lag increases with increasing slab thickness ($10\,\mu\mathrm{m}\leqslant L\leqslant 1$ mm) whereas the amplitude first increases and then decreases. This behavior is the result of superposition and interference of scattered photons from the bulk of the slab and from the back interface in forming the DPDW field at the front surface: As the thickness of the slab increases within the range of the scattering length, the number of back-scattered photons that contribute to the DPDW field at the front surface also increases because the total number of photons remaining in the slab and not escaping through transmission increases. The phase exhibits an increased lag because the center-of-mass of the depth-decaying diffuse-photon-field distribution (defined as the "*optical centroid*") shifts further into the body of the thicker turbid slab. With increasing thickness, however, the substantial contribution of the backscattered (coherent and diffuse) photons from the rear surface to the coordinate point (0,0) to the front-surface field decreases as the slab assumes the optically semi-infinite configuration. Therefore, the amplitude of the DPDW field at the front surface decreases and saturates, while the phase lag continues to increase and, eventually, saturates at very high frequencies (>100 MHz). The thermal-wave field at the surface of the slab corresponding to this DPDW distribution is shown in Fig. 3(b). It is seen that the order of amplitudes reflects the strength of the optical field in each case, Fig. 3(a) with the additional feature of the familiar [46] monotonic amplitude decrease with increasing frequency due to the decreasing thermal energy content per modulation period. The effect of the finite thickness of the medium on the thermal-wave phase is apparent in Fig. 3(b), where the optical centroid generally determines the relative thermal-wave phase lag, Fig. 3(a). However, the thermal-wave phase assumes the semi-infinite medium behavior at much lower frequencies ($f\geqslant 1$ kHz). Interference patterns resulting from the spatial confinement of thermal waves in thin layers [47] are apparent in the phase frequency response and tend to scramble the order of the DPDW phases. Figure 4 shows the interference of these DPDW and thermal-wave fields as a function of slab thickness for several values of μ_α. The amplitudes decrease with increasing optical absorption coefficient, as expected intuitively from enhanced nonradiative decay, Eq. (33). An optical interference maximum appears at slab thicknesses where the optical scattering length equals the thickness of the slab. Phase lags exhibit similar maxima at locations where the DPDW centroid shift deeper into the medium with increasing thickness is counterbalanced by the diminishing contributions of back-scattered photons (both coherent and diffuse) from the rear surface. Larger phase lags are associated with longer optical absorption depths, μ_α^{-1}, because photons can travel a longer distance before becoming absorbed. Figure 4(b) shows that the associated thermal-wave field depends on thickness in a manner similar to the distributed diffusive optical source. Here the order of the curves is, however, reversed from that of the DPDW field, since higher absorption means enhanced nonradiative decay and a correspondingly stronger thermal-wave TW field amplitude. The phase-lag order is also reversed, since larger μ_α results in enhanced thermal generation near the surface due to direct absorption events, rather than due to back-scattered photon absorption. This results in domination of the TW field by heat conduction processes to the bulk, thus shifting the thermal-wave centroid deeper into the body of the medium than near-surface localized back-scattered nonradiative photon-decay events. At the same time, saturation into the semi-infinite configuration for both amplitude and phase in Fig. 4(b) is achieved at shorter thicknesses with increasing μ_α, as the extent of the optical source in the bulk of the medium that contributes to the TW field decreases, and the TW distribution begins to dominate the thermal depth profile. Figure 5 shows the thickness dependence of the fields with the scattering coefficient μ_s as a parameter. Photon interference phenomena, similar to those in Fig. 4(a) are evident for all values of $\mu_s>0$, including nonzero phase lags. It is interesting to note that scattering strongly enhances the DPDW field at all slab thicknesses, with field amplitude at $\mathbf{r}=(0,0)$ monotonically increasing with increasing μ_s. The position of the maxima in both amplitude and phase is determined by the condition $\mu_s^{-1}\sim L$; therefore, a shift of the maximum to shorter thicknesses with increasing μ_s is observed in both amplitude and phase. The effects of the DPDW distributions on the TW field distribution are shown in Fig. 5(b). Scattered photons clearly represent an additional thermal-wave source at the front surface as the TW amplitude rises significantly with increasing μ_s. The nonscattering sample exhibits by far the lowest amplitude, as the forward propagating photons of the transparent medium contribute little to the surface thermal-wave field. The maxima of the amplitude are determined by the scattered photon interference pattern and appear at the same thicknesses as those of Fig. 5(a). The TW phase for $\mu_s=0$ does exhibit a small interference maximum due to the fact that infinite interreflections of the coherent optical beam localize the thermal-wave centroid at a depth>0 [37]. As μ_s increases from zero, the interplay between the thermal-wave generated by the forward coherent beam and the back-scattered photon field creates the oscillatory feature in the phase of Fig. 5(b) and the overall phase lag semi-infinite saturation value becomes dominated by the scattered field centroid which lies closer to the front surface: therefore, phase saturation at a smaller lag value than the coherent-only phase appears, consistently with Fig. 4(b). When scattering is further increased, however, substantial scattered photon den-

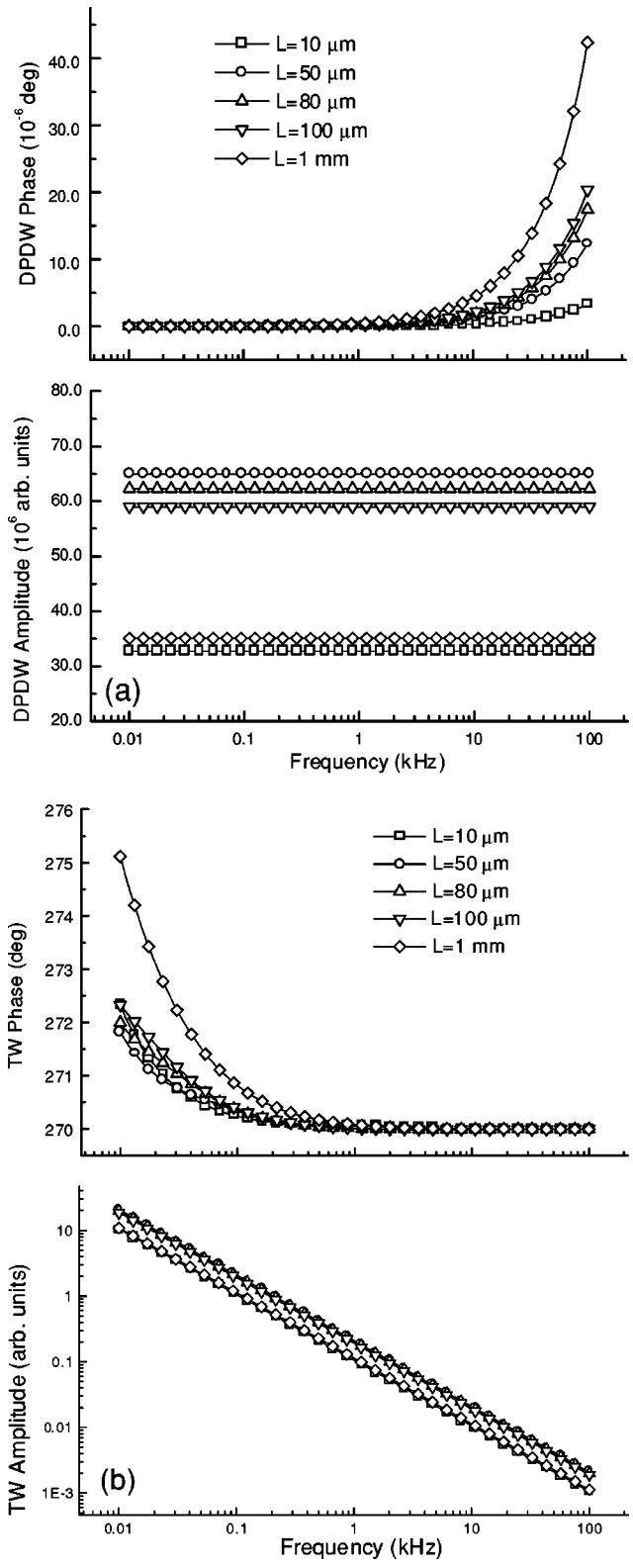

FIG. 3. Amplitude and phase of frequency response of (a) DPDW field, $\psi_t(0,0;\omega)$ and (b) associated thermal-wave field, $T(0,0;\omega)$, in a slab of variable thickness L of a turbid medium. Laser spotsize $W=0.48$ mm, $g=0.965$, $\xi=3.517$, $\mu_a=0.1\ \mathrm{mm}^{-1}$, and $\mu_s=31.8\ \mathrm{mm}^{-1}$. Thermophysical parameters: $\alpha=0.9\times10^{-7}\ \mathrm{m}^2/\mathrm{s}$, $k_t=0.446$ W/mK, $h=0$ (thermally insulating surfaces).

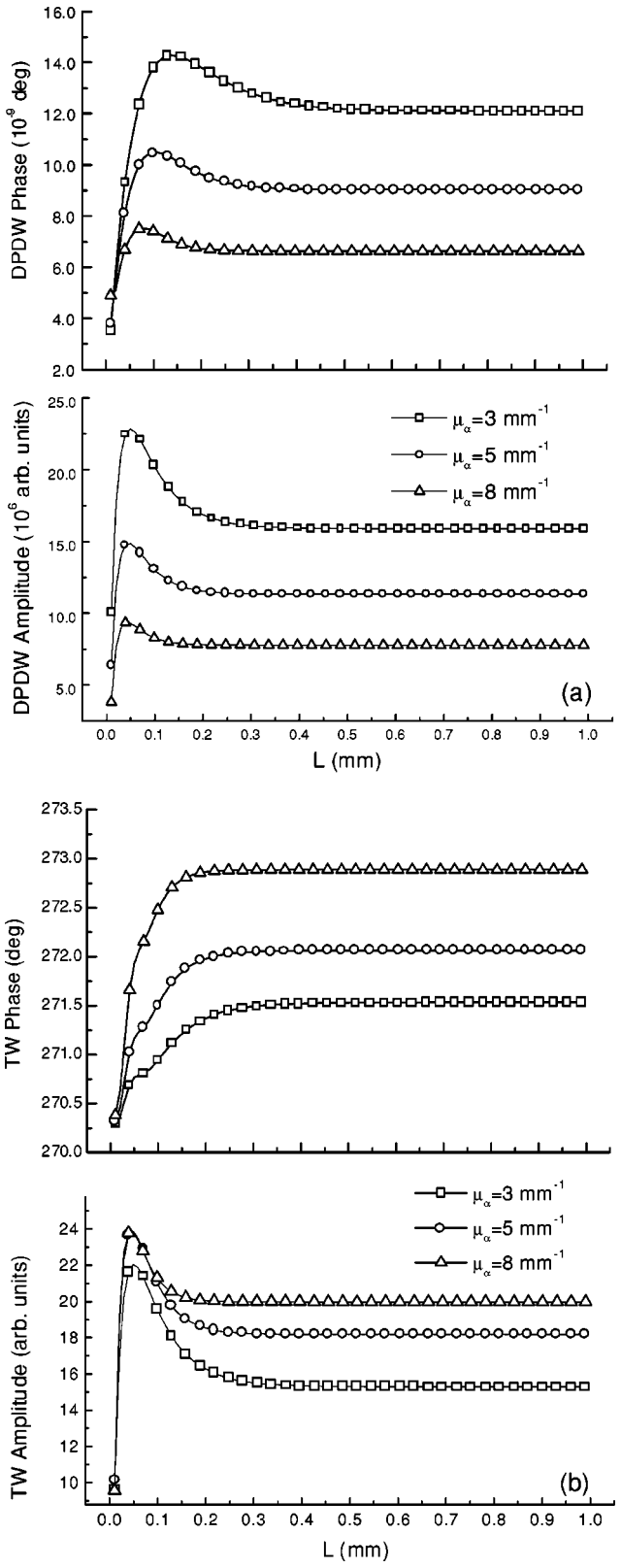

FIG. 4. Amplitude and phase thickness dependence of (a) DPDW field, $\psi_t(0,0;\omega)$ and (b) associated thermal-wave field, $T(0,0;\omega)$, in a slab of variable μ_a in a turbid slab. Laser spotsize $W=0.48$ mm, $g=0.965$, $\xi=3.517$, $f=100$ Hz, and $\mu_s=31.8\ \mathrm{mm}^{-1}$. Thermophysical parameters: $\alpha=0.9\times10^{-7}\ \mathrm{m}^2/\mathrm{s}$, $k_t=0.446$ W/mK, $h=0$ (thermally insulating surfaces).

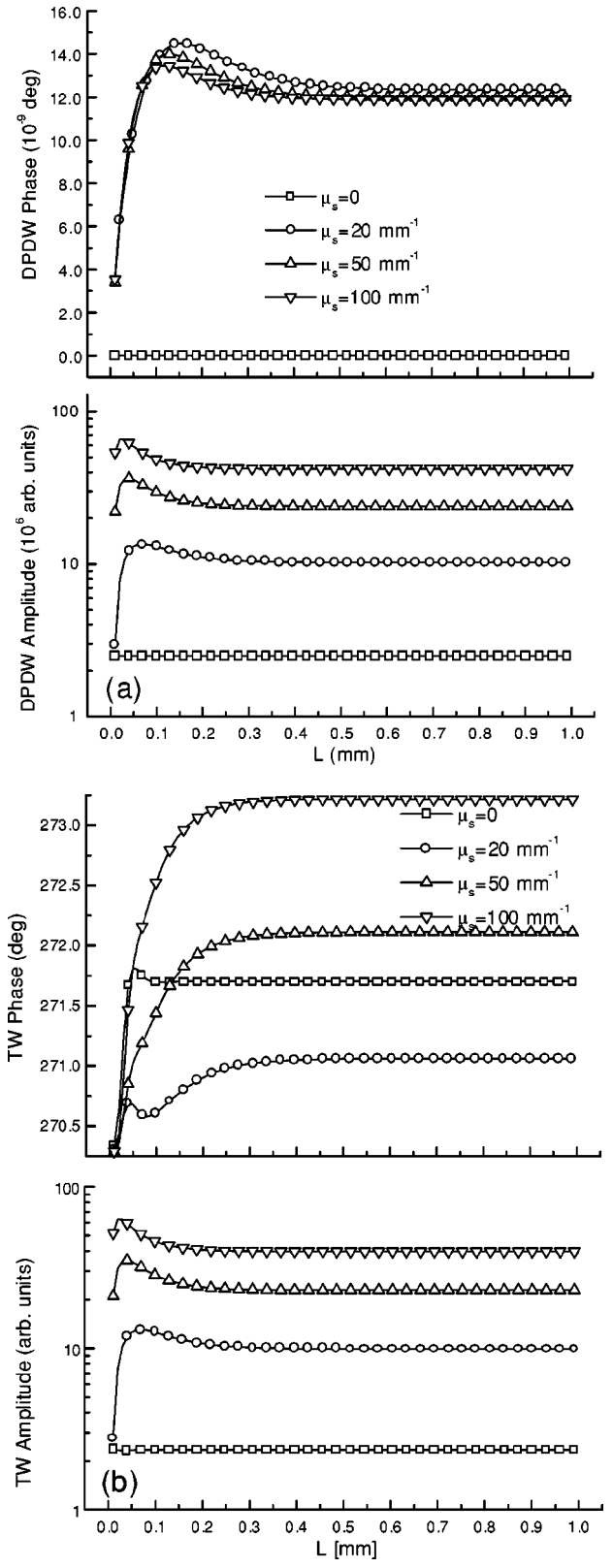

FIG. 5. Amplitude and phase thickness dependence of (a) DPDW field, $\psi_t(0,0;\omega)$and (b) associated thermal-wave field, $T(0,0;\omega)$, in a slab of variable μ_s of a turbid medium. Laser spot-size $W=0.48$ mm, $g=0.965$, $\xi=3.517$, $f=100$ Hz, and $\mu_a=3.0\,\mathrm{mm}^{-1}$. Thermophysical parameters: $\alpha=0.9\times10^{-7}\,\mathrm{m}^2/\mathrm{s}$, $k_t=0.446$ W/mK, $h=0$ (thermally insulating surfaces).

sities and the concomitant (nonradiative) heat generation occurs at deeper locations in the body of the turbid medium. Consequently, the saturation TW phase lag increases with μ_s. When the thickness of the turbid medium is fixed, an increased μ_a leads to decreasing DPDW amplitude as a result of enhanced optical-to-thermal energy conversion. It also leads to a decreased phase lag due to the steeper decay of the optical field closer to the front surface, Fig. 6(a). The associated TW field at the surface coordinate (0,0) and the PTR signal $U(r,\omega)$ the inverse Hankel transform of Eq. (49), both exhibit similar behavior dominated by trends in Fig. 6(a), as shown in Fig. 6(b). The (TW and) PTR amplitude increases monotonically with increasing μ_a, and it decreases with increasing modulation frequency as the thermal-wave energy imparted to the slab over one period decreases. Furthermore, the phase lag increases with increasing μ_a for the same reasons as in Fig. 4(b). All PTR phases saturate to the same value at high frequencies (thermally thick limit [48]), because in that limit it is the thermal diffusion length, $L_d(\omega)=|\sigma_t|^{-1}$ that determines the extent of the TW centroid in the bulk of the turbid medium and not the optical absorption or scattering lengths. Since σ_t, Eq. (36) depends on the (common) thermal diffusivity, all phase curves in Fig. 6(b) saturate at the same value above ca. 1 kHz.

Finally, the effects of the heat transfer coefficient h on the TW and PTR fields generated by the DPDW field in a turbid medium can be substantial. Figure 7 shows a simulated case of a 9-mm-thick turbid slab, in which h varies over several orders of magnitude. The TW amplitude at (0,0) decreases with increasing h, as more thermal energy escapes into the ambient through interfacial transport at both front and back surfaces. As frequency increases, the back surface heat losses become less significant in determining the TW amplitude of the front-surface and all curves converge together. Similar trends are observed in the phases: As h increases, the TW centroid shifts closer to the front surface due to heat losses there, thus decreasing the overall phase lag. However, at high frequencies, the (common) thermal diffusion length is shorter than the thermal energy depletion depth (k_t/h) and dominates the phase lag; therefore, all phases tend to saturate at the same value. The behavior of the PTR signal is significantly different from that of the $\psi_t(0,0;\omega)$ as the computation of the former involves a depth integral over the thickness of the turbid medium. As a result, the PTR amplitudes, Fig. 7(b), are more sensitive to thermal-wave interference phenomena [47] within the body of the finitely-thick slab at low frequencies (thermally thin limit). At high frequencies, the PTR amplitudes are controlled by the (common) thermal diffusion length, and all curves converge to a single value. The PTR phases exhibit h-dependent minima, which shift to higher frequencies with increasing value of h. The occurrence of these extrema is due to the fact that the PTR phase is determined by two counteracting mechanisms: the thermal losses at the front surface, which tend to localize the TW field closer to that surface, and the position of the TW centroid due to heat diffusion to the bulk, which tends to shift the phase away from the surface. As h increases, the former mechanism becomes more important and the composite TW centroid, essentially given by $L_c(\omega)=1/[\sigma_t(\omega)$

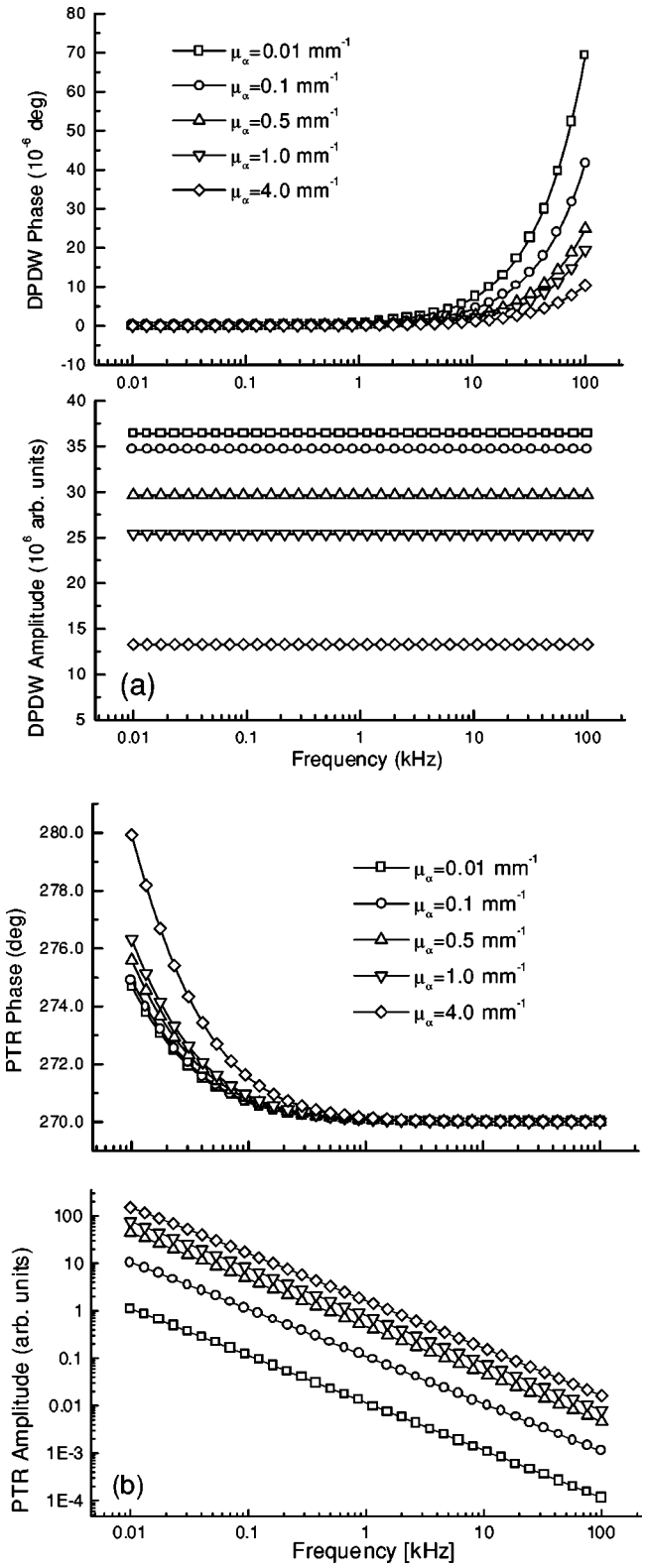

FIG. 6. Amplitude and phase thickness dependence of (a) DPDW field, $\psi_t(0,0;\omega)$ and (b) the associated PTR field, $U(0,\omega)$, in a slab of variable μ_a of a turbid medium. Laser spotsize $W=0.48$ mm, $g=0.965$, $\xi=3.517$, and $L=0.9$ cm. Thermophysical parameters: $\alpha=0.9\times10^{-7}$ m^2/s, $k_t=0.446$ W/mK, $h=0$ (thermally insulating surfaces). $\overline{\mu}_{\rm IR}=60$ mm^{-1}.

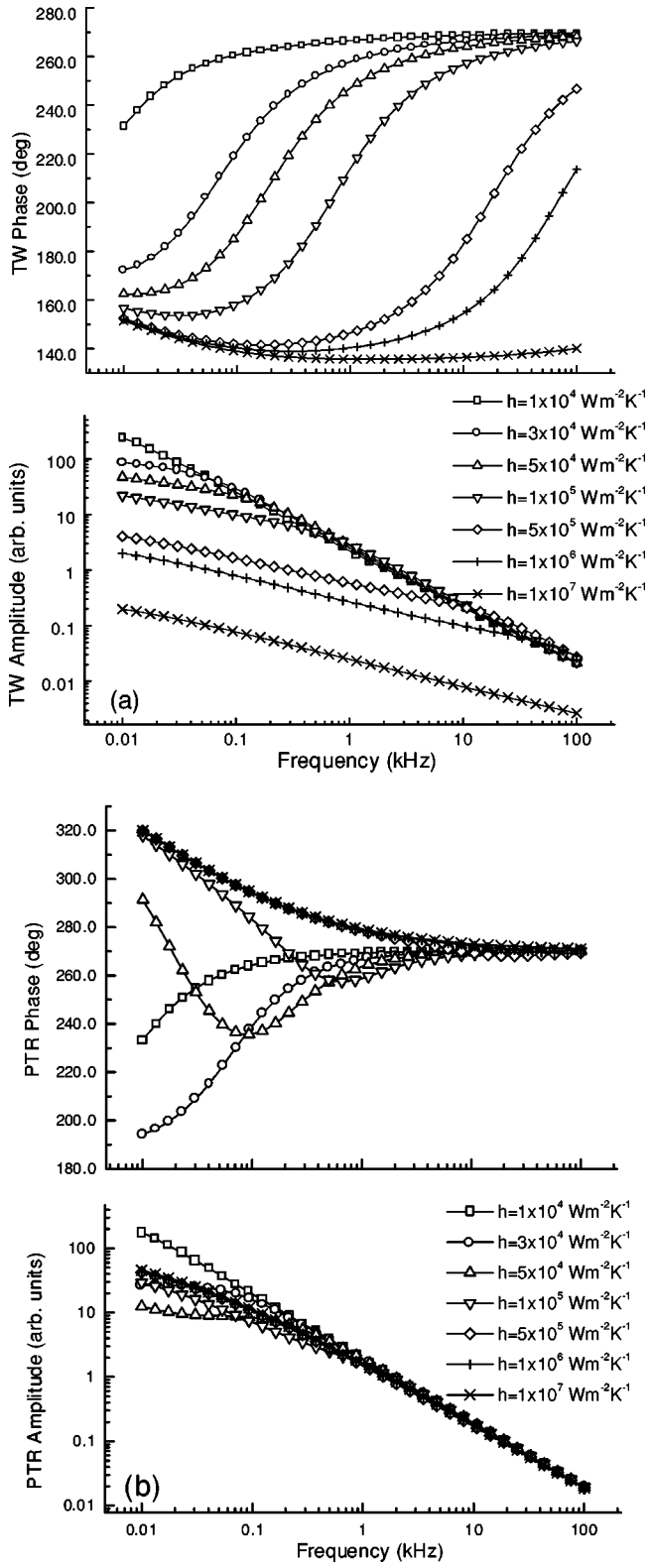

FIG. 7. Amplitude and phase thickness dependence of (a) DPDW field, $\psi_t(0,0;\omega)$ and (b) the associated PTR field, $U(0,\omega)$, in a slab of a turbid medium as a function of modulation frequency, with h as a parameter. Laser spotsize $W=0.48$ mm, $g=0.965$, $\xi=3.517$, $\mu_a=11.8$ mm^{-1}, $\mu_s=31.8$ mm^{-1}, and $L=0.9$ cm. Thermophysical parameters: $\alpha=0.9\times10^{-7}$ m^2/s, $k_t=0.446$ W/mK, $\overline{\mu}_{\rm IR}=60$ mm^{-1}.

$+(h/k_t)]$, shifts closer to the front surface, thus shifting the phase extremum to higher frequencies.

B. Dependence on depth coordinate in a turbid medium

In view of the fact that the diffusion approximation of the photon density-wave field may not be strictly applicable at the surface of a scattering medium [18] within the ballistic photon regime, some simulations were performed as a function of depth in a slab of a turbid medium to study the behavior of this approximation within shallow depths commensurate with the optical scattering length, μ_s^{-1}. Figure 8(a) shows several DPDW depth profiles with μ_s as a variable parameter. The photon-density profile at $\mathbf{r}=(0,0)$ increases with increasing scattering coefficient value, as the result of contributions from scattered photons to the axial DPDW field. This result is consistent with the earlier calculations shown in Fig. 5. The amplitude curves decrease into the medium for large values of μ_s as smaller photon densities can be sustained inside intensely scattering media. The DPDW phase lag increases with increasing μ_s, because photons scattered farther away from the front surface are likely to contribute to the axial value of the field thus shifting the optical centroid farther away from the laser incidence coordinate. The phase lag increases with increasing z value are due to the localization of the photon-density centroid near the surface and within ca. one scattering length, μ_s^{-1}: it is easy to see in Fig. 8(a) that the flat range of the phase curves starting at the surface decreases with increasing μ_s. Ishimaru *et al.* [16] have reported similar trends in measurements of transmitted optical power through randomly distributed particles (latex scatterers) of sizes 0.109 and 2.02 μm. The TW field amplitude depth profile, Fig. 8(b), is determined by the associated DPDW depth profile, Fig. 8(a), which acts as the oscillating temperature source. The TW phase exhibits very shallow near-surface maxima, which become sharper and shift to shallower z locations with increasing μ_s. No discernible maximum is observed for $\mu_s < 30\,\mathrm{mm}^{-1}$. These phase-lag maxima appear as a result of the trade off between enhanced near-surface optical source contributions (within a depth μ_s^{-1}) with increasing scattering coefficient, and the much deeper thermal-wave centroid due to the optical absorption depth μ_a^{-1}. Given that in turbid tissue $\mu_s > \mu_a$, past the subsurface location of the scattering centroid, the phase lag is determined by μ_a^{-1}. All phases eventually coincide as the depth equal to $\mu_a^{-1}=100\,\mathrm{mm}$ is approached; those from media with larger scattering coefficients saturate more readily to the μ_a-dominated value with increasing depth (i.e., with relatively steeper rates of phase change $d\phi/dz$), due to the shorter scattering length about the scattering centroid. Furthermore, fewer photons survive scattering to contribute to the coherent transmitted axial beam and the TW amplitude decreases more steeply as a function of depth in this case. To complete the physical picture, a depth-profilometric simulation with the optical absorption coefficient as a parameter and $\mu_s=100\,\mathrm{mm}^{-1}$ was also worked out. The DPDW field behavior is shown in Fig. 9(a). In agreement with trends in Fig. 4(a) the amplitude decreases with increasing μ_a for fixed depth coordinate due to the enhanced nonradiative de-excitation rate that diminishes the number density of available photons. Furthermore, the rate of amplitude decrease with depth increases with increasing value of μ_a, as intuitively expected. The DPDW phase lags are larger for smaller μ_a values as the optical field extends farther away from the location of its incidence on the turbid medium [see also the phases in Fig. 4(a)]. The associated TW amplitude, Fig. 9(b), exhibits cross overs at certain characteristic depths, z_μ. For $z<z_\mu$, higher values of μ_a create stronger thermal-wave fields; however, less optical power is transmitted deeper into the medium, with the result that the TW field drops off more sharply as a function of increasing z. Conversely, more transparent media can sustain stronger optical fields than more opaque media at greater depths. The result is the observed cross-over behavior. The peaks of the TW phases in Fig. 9(b) are fixed by the (common) value of $\mu_s^{-1}=0.01\,\mathrm{mm}$, whereas the phase cross overs are consistent with the foregoing amplitude crossover mechanism: for depths $z<z_\mu$ the media with larger optical absorption coefficients, exhibit greater phase lags as heat conduction into deeper regions dominates the thermal-wave centroid; for depths $z>z_\mu$, however, the optical absorption depth, μ_a^{-1} dominates the phase lag, which becomes larger for more transparent media.

Finally, in view of the criticism of the validity of the present photon-diffusion-wave theoretical formalism within the ballistic photon region, the ''skin layer,'' [21,22] the foregoing simulations of the depth dependence of the DPDW field profiles demonstrate only mild depth dependences within the typical photon scattering lengths $0.0067\,\mathrm{mm} \leqslant \mu_s^{-1} \leqslant 0.05\,\mathrm{mm}$. Therefore, it can be deduced that the present theoretical formalism can yield accurate descriptions of physical processes up to subsurface regions within 7–50 μm from the illuminated surface. Within the ballistic-photon boundary layer the physical necessity for diffuse power conservation at the interface embodied in the boundary conditions Eqs. (8) and (9), as well as the relatively flat near-surface behavior of Figs. 8 and 9, render the predictions of these plots plausible approximations of the actual photon-field behavior in that layer. The PTR signals are expected to be even more reliably predictable by curves such as those in Figs. 8(b) and 9(b), since the very thin boundary skin layer represents only a small fraction of the depth-integrated signal according to Eq. (48).

C. Dependence on μ_a and μ_s of a turbid medium

The simulations shown in Figs. 4, 6, and 9 have indicated that the DPDW field amplitude decreases with increasing value of μ_a and the phase lag also decreases. This is the result of the higher spatial confinement of the photon field near the laser source with increased optical absorption coefficients. At the same time the TW field amplitude increases due to the enhanced conversion rate of photons into heat. The phase lag increases as the increased strength of the TW source penetrates deeper layers in the body of the medium through conduction heat transfer from the near-surface region. Figure 10 shows another aspect of this behavior as a function of μ_a for a highly scattering tissue-type medium. It

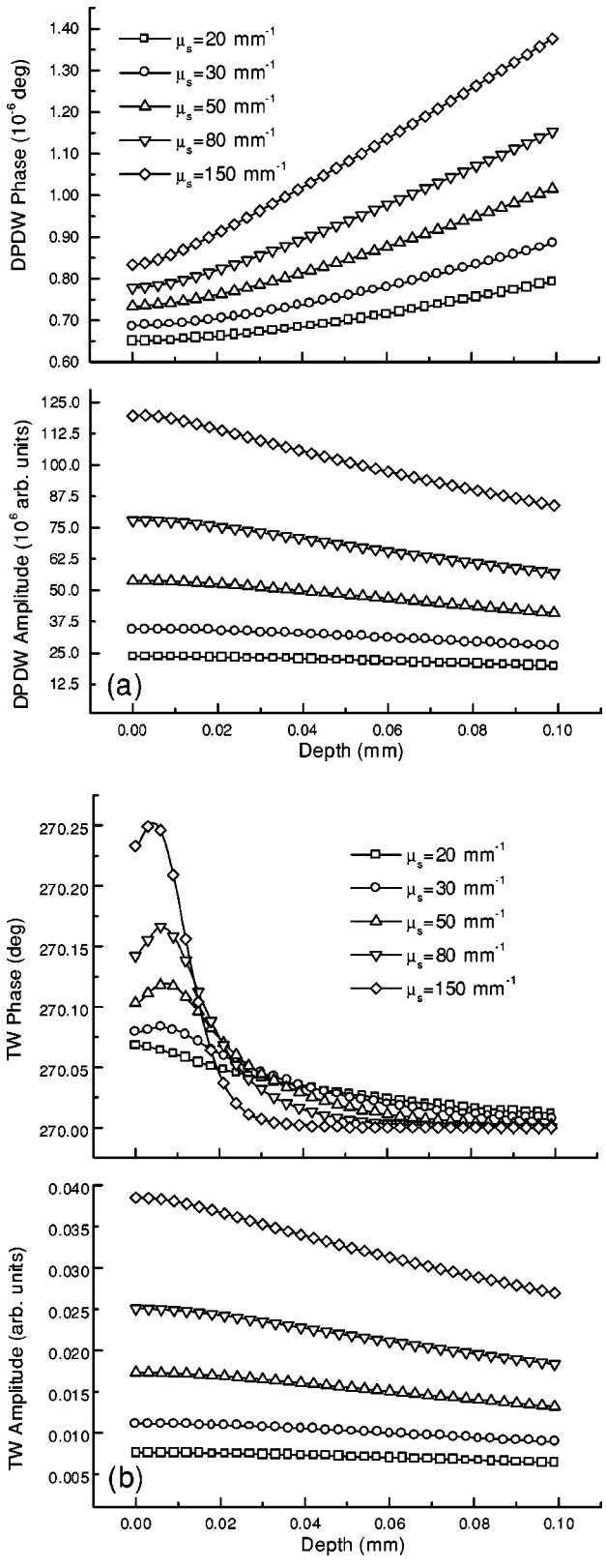

FIG. 8. Amplitude and phase depth dependence of (a) DPDW field, $\psi_t(0,0;\omega)$ and (b) associated thermal-wave field, $T(0,0;\omega)$, in a slab of a turbid medium of variable μ_s. Laser spotsize $W=0.48$ mm, $g=0.965$, $\xi=3.517$, $f=1$ kHz, and $\mu_a=0.01\,\mathrm{mm}^{-1}$. Thermophysical parameters: $\alpha=0.9\times10^{-7}\,\mathrm{m}^2/\mathrm{s}$, $k_t=0.446$ W/mK, $h=0$ (thermally insulating surfaces).

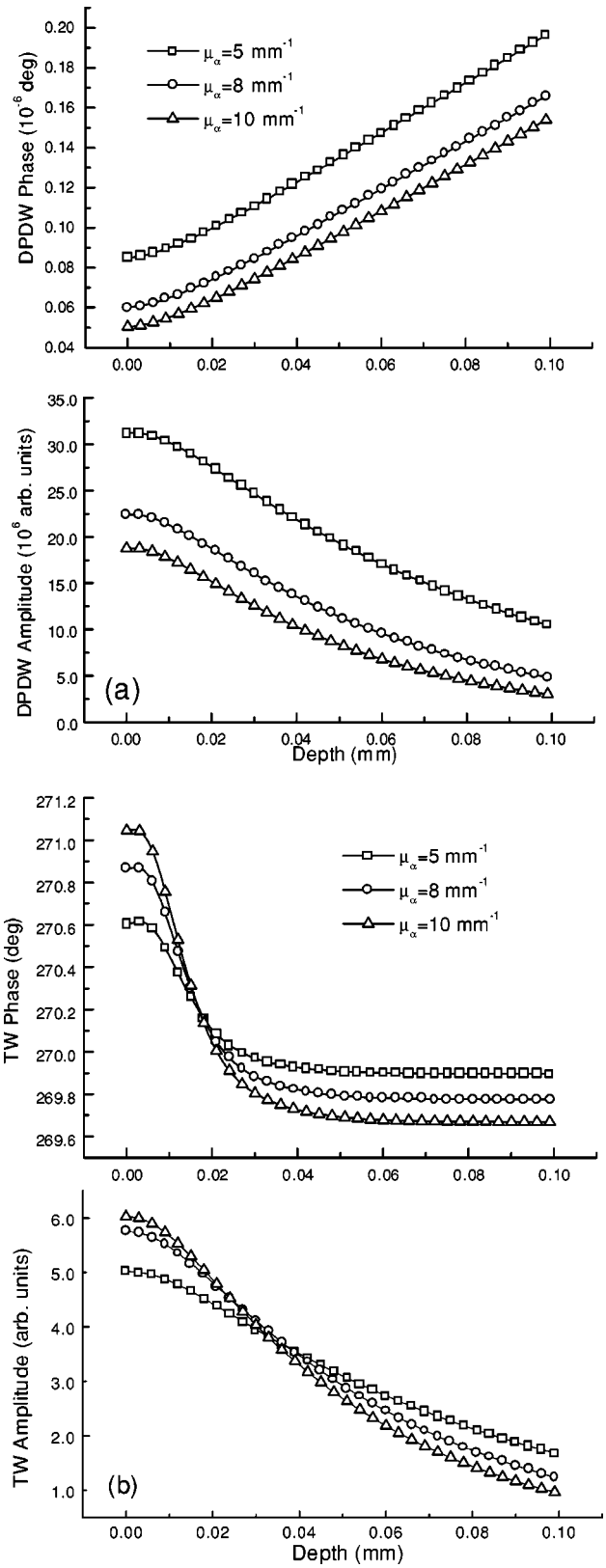

FIG. 9. Amplitude and phase depth dependence of (a) DPDW field, $\psi_t(0,0;\omega)$ and (b) associated thermal-wave field, $T(0,0;\omega)$, in a slab of a turbid medium of variable μ_a. Laser spotsize $W=0.48$ mm, $g=0.965$, $\xi=3.517$, $f=1$ kHz, and $\mu_s=100\,\mathrm{mm}^{-1}$. Thermophysical parameters: $\alpha=0.9\times10^{-7}\,\mathrm{m}^2/\mathrm{s}$, $k_t=0.446$ W/mK, $h=0$ (thermally insulating surfaces).

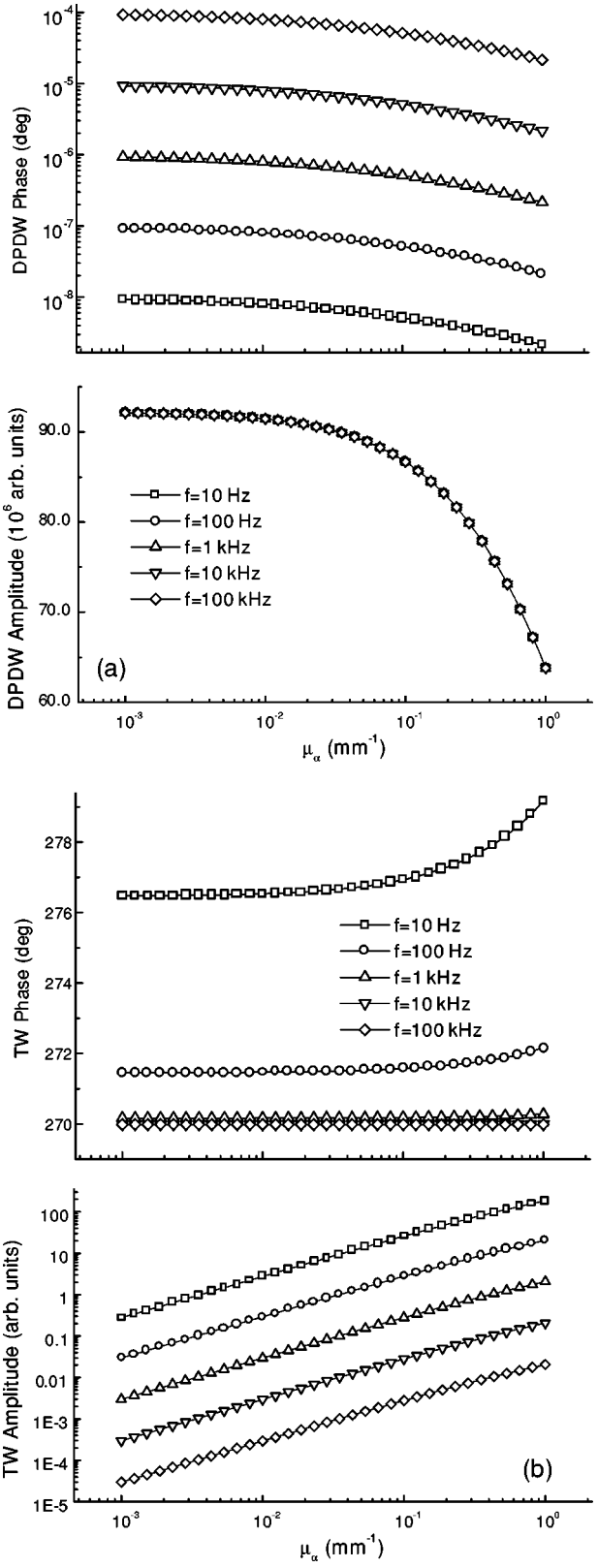

FIG. 10. Amplitude and phase dependence on μ_a of (a) DPDW field, $\psi_t(0,0;\omega)$ and (b) associated thermal-wave field, $T(0,0;\omega)$, in a slab of a turbid medium of variable modulation frequency f. Laser spotsize $W=0.48$ mm, $g=0.965$, $\xi=3.517$, $L=0.9$ cm, and $\mu_s=100\,\mathrm{mm}^{-1}$. Thermophysical parameters: $\alpha=0.9\times10^{-7}\,\mathrm{m}^2/\mathrm{s}$, $k_t=0.446$ W/mK, $h=0$ (thermally insulating surfaces).

is seen that modulation frequency up to 100 kHz has no effect on the DPDW amplitude, which is entirely dominated by μ_s and essentially independent of μ_a for values of this parameter up to 0.01 mm^{-1}. The DPDW phase, however, increases dramatically with frequency, as the factor $\omega\tau_a$ of the complex wave number, Eq. (7), changes rapidly, giving rise to larger contributions to the imaginary part of the field. Therefore, the turbid medium may be said to transition from the photon-wave thin to the photon-wave thick regime above source modulation frequencies greater than $f_0\sim 1/2\pi\tau_a$. Of course, the overall DPDW phase remains extremely small (experimentally until the modulation frequency f_0 is attained). For diffuse-photon migration this frequency is in the >100 MHz range [44,45]. Figure 10(b) is the associated TW response: The amplitude decreases monotonically with increasing frequency, as expected from the decreased thermal energy content in each period. It also increases with increasing μ_a consistently with the complementary nature of the DPDW and TW field intensities, a result of the enhanced photon-to-heat conversion rate. The phase lag decreases with increasing frequency due to increased localization of the TW field near the source coordinate; it also increases with increasing μ_a, for the same reasons as the TW phase at shallow depths in Fig. 9(b). Figure 11 shows simulations of the μ_a dependence of the front-surface DPDW and TW fields with the coefficient μ_s as a parameter. As in the case of Figs. 5 and 8, increasing μ_s enhances the photon-density amplitude as statistically more photons from all directions get scattered back into the observation coordinate $\mathbf{r}$. Similarly, the phase lag increases with increasing μ_s, as the enhanced scattering process moves the optical centroid away from the source coordinate. The amplitude of the TW response in Fig. 11(b) exhibits the expected correlation with the DPDW amplitude, as enhanced scattering amounts to a more intense local optical field and thus increased nonradiative conversion rate. The monotonic increase of the TW amplitude with μ_a is consistent with that in Fig. 10(b). The TW phase lag of Fig. 11(b) increases with increasing μ_s, as expected from the behavior of the associated DPDW phase of Fig. 11(a), since scattering (and not absorption) dominates the source of the TW field. The phase dependence on μ_a is quite small, but physically insightfull: For relatively small values of μ_s the spatial confinement of the local thermal-wave field due to the increased μ_a dominates the thermal behavior; as a result the phase lag decreases for high μ_a. For values of $\mu_s>30\,\mathrm{mm}^{-1}$, the photon-scattering-dominated optical centroid dominates the TW source and moves away from the source coordinate, thus increasing the TW phase lag. Figure 12 clearly shows the trade off between increases of the DPDW field amplitude and phase lag with increasing μ_s, and decreases in the respective quantities (without change in curve shapes) with increasing μ_a. It is noted that the steep increase at low μ_s is followed by near-saturation conditions for $\mu_s\gtrsim 400\,\mathrm{mm}^{-1}$ (diffuse-photon saturation), as the enhanced scattering ''shields'' the observation (source) coordinate $\mathbf{r}=(0,0)$ from further contributions from remotely scattered photons, thus limiting any further shift of the optical centroid away from it. The much greater impact of changing μ_a on the associated PTR amplitude is seen in Fig. 12(b),

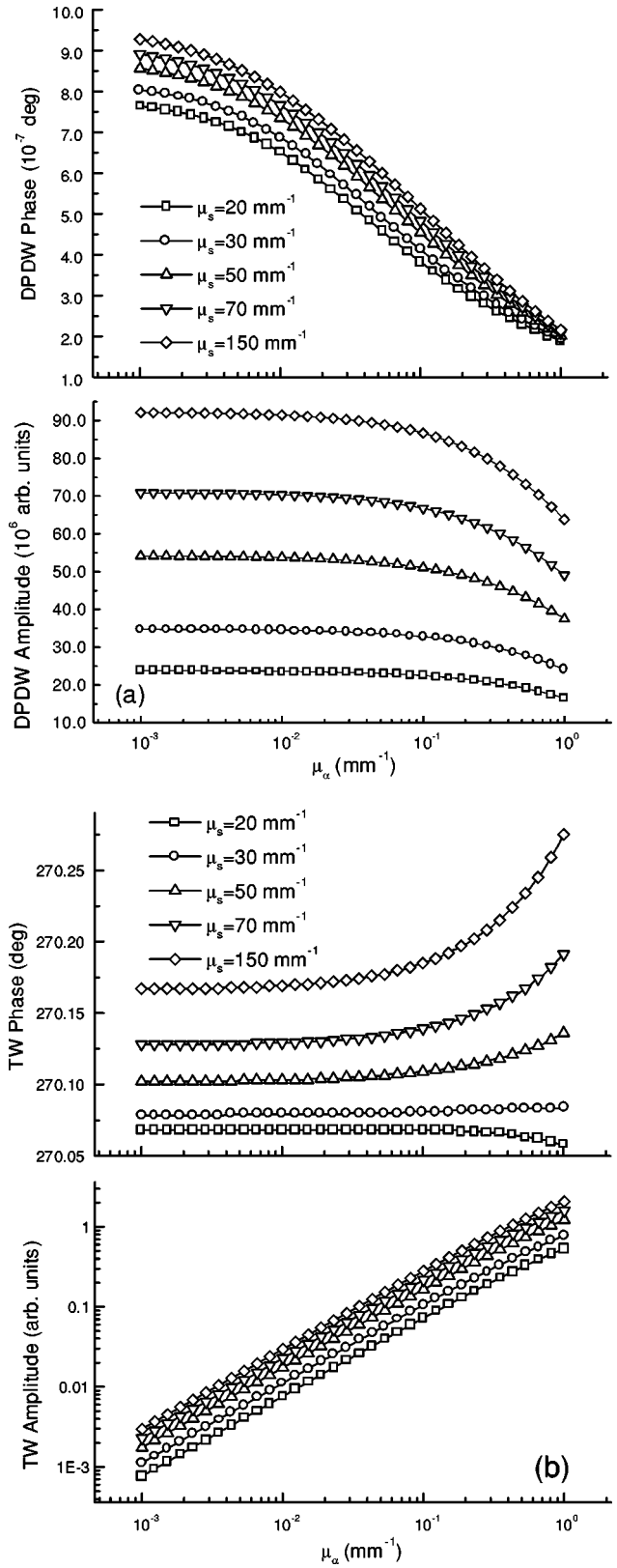

FIG. 11. Amplitude and phase dependence on the coefficient μ_a of (a) DPDW field, $\psi_t(0,0;\omega)$ and (b) associated thermal-wave field, $T(0,0;\omega)$, in a slab of a turbid medium of variable μ_s. Laser spotsize $W=0.48$ mm, $g=0.965$, $\xi=3.517$, $L=0.9$ cm, and $f=1$ kHz. Thermophysical parameters: $\alpha=0.9\times10^{-7}$ m^2/s, $k_t=0.446$ W/mK, $h=0$ (thermally insulating surfaces).

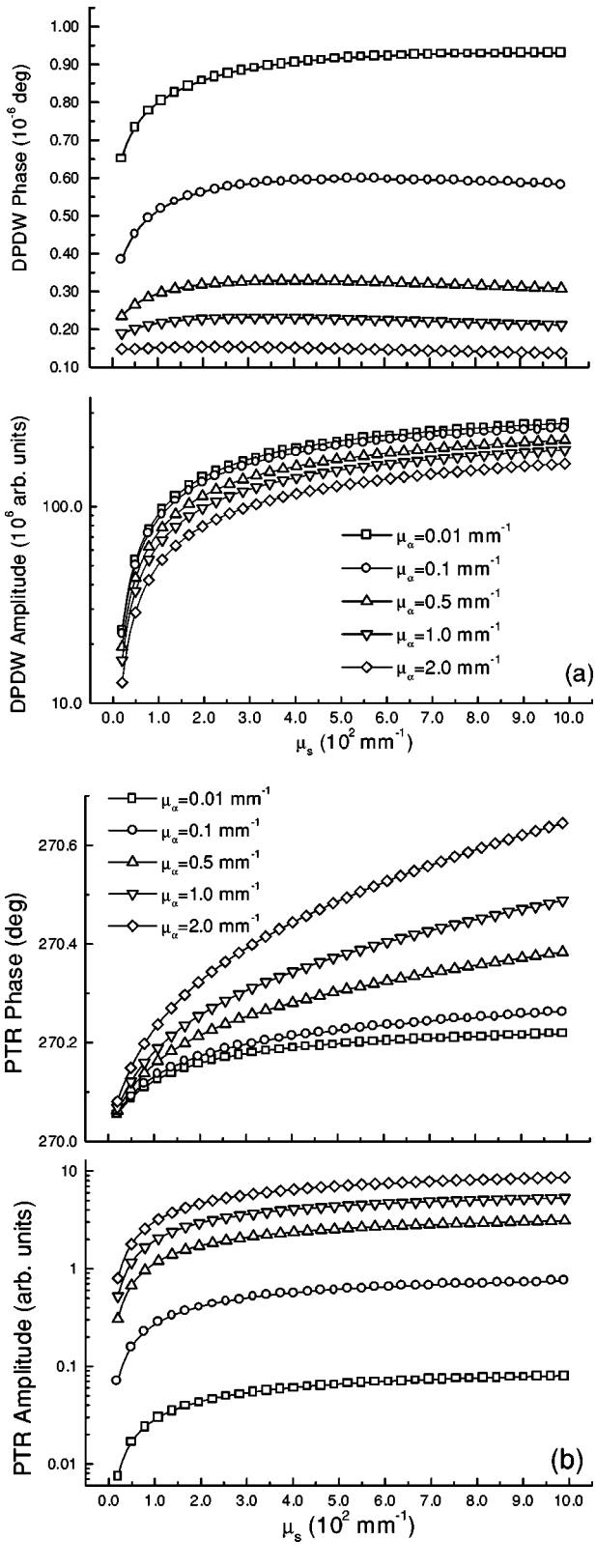

FIG. 12. Amplitude and phase dependence on μ_s of (a) DPDW field, $\psi_t(0,0;\omega)$ and (b) the associated PTR field, $U(0,\omega)$, in a slab of a turbid medium as a function of modulation frequency, with μ_a as a parameter. Laser spotsize $W=0.48$ mm, $g=0.965$, $\xi=3.517$, $f=1$ kHz, and $L=0.9$ cm. Thermophysical parameters: $\alpha=0.9\times10^{-7}$ m^2/s, $k_t=0.446$ W/mK, and $h=0$. $\overline{\mu}_{\rm IR}=60$ mm^{-1}.

where the depth integration of the TW field preserves and accelerates the gradual diffuse-photon saturation with increasing μ_s. Yasa, Jackson, and Amer [46] and Helander and Lundstrom [49] have reported experimental verifications of this effect using photothermal methods. The PTR phase saturates more slowly because, as a result of depth integration, it is sensitive to the composite thermal centroid determined by all three values of μ_s^{-1}, μ_a^{-1}, and $\overline{\mu}_{\mathrm{IR}}^{-1}$. Therefore, the scattering component has only partial influence on the behavior of the phase with μ_s.

VIII. CONCLUSIONS

A three-dimensional theory of the frequency-domain thermal-wave field generated inside a turbid medium with optical and thermal properties of human tissue has been presented. The optical source was treated as a Gaussian-laser-beam-excited three-dimensional harmonically modulated diffuse photon-density-wave (DPDW) field in the diffusion approximation of the radiative transfer theory. Numerical inversions of the derived spatial Hankel transforms were performed to study the dependence of the DPDW field and of the associated thermal-wave field or photothermal radiometric signal on the key parameters of turbid media, such as the optical absorption and optical scattering coefficients, modulation frequency, sample thickness, and optical or photothermal depth profile. The derived theory can be used toward computational multiparameter fits of experimental data using frequency-domain photothermal radiometry or other photothermal techniques probing turbid media. Preliminary applications of the present theory to soft tissue phantoms [42] and dental enamel [50] (the latter used as an example of nonzero lifetime-limited fluorescent turbid optical medium) have already shown very good promise with regard to the ability of the theory to measure the reduced optical scattering and absorption coefficients of these media uniquely and within 20% and 10%, respectively, of the values independently derived by using Mie theory and spectrophotometric measurements.

ACKNOWLEDGMENTS

The authors wish to acknowledge useful discussions with, and valuable comments by, Dr. Alex Vitkin, Princess Margaret Hospital, Toronto, on some aspects of the theoretical formalism. The contribution of Lena Nicolaides with an early version [42] of the improper integral routine *qromo* [41] is also acknowledged. The support of the Natural Sciences and Engineering Research Council of Canada (NSERC) to one of us (C.F.) is gratefully acknowledged.

[1] *Photon Migration in Tissues*, edited by B. Chance (Plenum, New York, 1989).
[2] *Optical-Thermal Response of Laser-Irradiated Tissue*, edited by A. J. Welch and M. J. C. van Gemert (Plenum, New York, 1995).
[3] W. F. Cheong, S. A. Prahl, and A. J. Welch, IEEE J. Quantum Electron. **26**, 2166 (1990).
[4] S. R. Arridge, P. van der Zee, M. Cope, and D. T. Delpy, Proc. SPIE **1431**, 204 (1991).
[5] B. C. Wilson, E. M. Sevick, M. S. Patterson, and B. Chance, Proc. IEEE **80**, 918 (1992).
[6] S. L. Jacques, J. S. Nelson, W. H. Wright, and T. E. Milner, Appl. Opt. **32**, 2439 (1993).
[7] S. A. Prahl, I. A. Vitkin, U. Bruggemann, B. C. Wilson, and R. R. Anderson, Phys. Med. Biol. **37**, 1203 (1992).
[8] S. A. Prahl, in *Progress in Photothermal and Photoacoustic Science and Technology*, edited by A. Mandelis and P. Hess (SPIE, Bellingham, WA, 1997), Vol. III, Chap. 11.
[9] T. E. Milner, D. M. Goodman, B. S. Tanenbaum, and J. S. Nelson, J. Opt. Soc. Am. A **12**, 1479 (1995).
[10] L. Nicolaides, A. Mandelis, and S. Abrams, J. Biomed. Opt. **5**, 31 (2000).
[11] L. Nicolaides, Y. Chen, A. Mandelis, and I. A. Vitkin, in Proceedings of the International Conference on Photoacoustic Photothermal Phenomena, Kyoto, 2000, edited by T. Sawada and M. Terazima [Anal. Sci. **17**, s326 (2000)].
[12] A. Yodh and B. Chance, Phys. Today **48** (3), 34 (1995).
[13] A. Mandelis, Phys. Today **53** (8-1), 29 (2000).
[14] A. Ishimaru, *Wave Propagation and Scattering in Random Media* (Academic, New York, 1978).
[15] J. A. Kang, *Electromagnetic Wave Theory* (Wiley, New York, 1986).
[16] E. Amic, J. M. Luck, and Th. M. Nieuwenhuizen, J. Phys. I **7**, 445 (1997); A. Ishimaru, Y. Kuga, R. L.-T. Cheung, and K. Shimizu, J. Opt. Soc. Am. **73**, 131 (1983).
[17] D. A. Boas and A. G. Yodh, J. Opt. Soc. Am. A **14**, 192 (1997).
[18] T. J. Farrell, M. S. Patterson, and B. Wilson, Med. Phys. **19**, 879 (1992).
[19] J. J. Doderstadt and L. J. Hamilton, *Nuclear Reactor Analysis* (Wiley, New York, 1976); R. C. Haskell, L. O. Svaasand, T.-T. Tsay, T. C. Feng, M. S. McAdams, and B. J. Tromberg, J. Opt. Soc. Am. A **11**, 2727 (1994).
[20] M. S. Patterson, in *Optical-Thermal Response of Laser-Irradiated Tissue*, edited by A. J. Welch and M. J. C. van Gemert (Plenum, New York, 1995).
[21] Th. M. Nieuwenhuizen and J. M. Luck, Phys. Rev. E **48**, 569 (1993).
[22] M. C. W. van Rossum and Th. M. Nieuwenhuizen, Rev. Mod. Phys. **71**, 313 (1999).
[23] A. Ishimaru, Appl. Opt. **28**, 2210 (1989).
[24] A. Mandelis, *Diffusion Wave Fields: Mathematical Methods and Green Functions* (Springer, New York, 2001), Chap. 10, pp. 662–672.
[25] M. Q. Brewster, *Thermal Radiative Transfer and Properties* (Wiley, New York, 1992), p. 407.
[26] G. Eason, R. Veich, R. Nisbet, and F. Turnbull, J. Phys. D **11**, 1463 (1978).
[27] W. M. Star and J. P. A. Marijnissen, J. Photochem. Photobiol., B **1**, 149 (1987).
[28] R. R. Anderson, H. Beck, U. Bruggemann, W. Farinelli, S. L.

Jacques, and J. Parrish, Appl. Opt. **28**, 2256 (1989), Eq. (8).
[29] R. A. J. Groenhuis, H. A. Ferwerda, and J. J. T. Bosch, Appl. Opt. **22**, 2456 (1983).
[30] M. Keijzer, W. M. Star, and P. R. Storchi, Appl. Opt. **27**, 1820 (1988).
[31] J. Vanniasinkam, A. Mandelis, M. Munidasa, and M. Kokta, J. Opt. Soc. Am. B **15**, 1647 (1998).
[32] B. Majaron, W. Verkruysse, B. S. Tanenbaum, T. E. Milner, and J. S. Nelson, in *Proceedings of the SPIE Biomedical Optics Society Conference, San Jose, CA, 2000* (SPIE, Bellingham, WA), Vol. 3907, p. 114.
[33] W. P. Leung and A. C. Tam, J. Appl. Phys. **56**, 153 (1984).
[34] B. J. Tromberg, S. Masden, C. Chapman, L. O. Svaasand, and R. C. Haskell, *Advances in Optical Imaging and Photon Migration* (Optical Society of America Press, Washington D.C., 1994), Vol. 21, p. 93.
[35] M. A. O'Leary, D. A. Boas, X. D. Li, B. Chance, and A. G. Yodh, Opt. Lett. **21**, 158 (1996).
[36] X. D. Li, M. A. O'Leary, D. A. Boas, B. Chance, and A. G. Yodh, Appl. Opt. **35**, 3746 (1996).
[37] A. Mandelis and J. Vanniasinkam, J. Appl. Phys. **80**, 6107 (1996).
[38] J. M. Schmidt, G. X. Zhou, E. C. Walker, and R. T. Wall, J. Opt. Soc. Am. A **7**, 2141 (1990).
[39] B. J. Tromberg, L. O. Svaasand, T.-T. Tsay, and R. C. Haskell, Appl. Opt. **32**, 607 (1993).
[40] M. S. Patterson, B. Chance, and B. C. Wilson, Appl. Opt. **28**, 2331 (1989).
[41] W. H. Press, S. A. Teukolsky, W. T. Vetterling, and B. P. Flannery, *Numerical Recipes in C*, 2nd ed. (Cambridge University Press, New York, 1992).
[42] L. Nicolaides, Y. Chen, A. Mandelis, and I. A. Vitkin, J. Opt. Soc. Am. A **18**, 2548 (2001).
[43] C. F. Bohren and D. R. Huffman, *Absorption and Scattering of Light by Small Particles* (Wiley, New York, 1983).
[44] J. R. Lakowicz and K. Berndt, Chem. Phys. Lett. **166**, 246 (1990).
[45] M. S. Patterson, J. D. Moulton, B. C. Wilson, K. W. Berndt, and J. R. Lakowicz, Appl. Opt. **30**, 4474 (1991).
[46] Z. A. Yasa, W. B. Jackson, and N. M. Amer, Appl. Opt. **21**, 21 (1982).
[47] C. A. Bennett and R. P. Patty, Appl. Opt. **21**, 49 (1982).
[48] A. Rosencwaig and A. Gersho, J. Appl. Phys. **47**, 64 (1976).
[49] P. Helander and I. Lundstrom, J. Appl. Phys. **51**, 3841 (1980).
[50] L. Nicolaides, C. Feng, and A. Mandelis, Appl. Opt. (to be published).